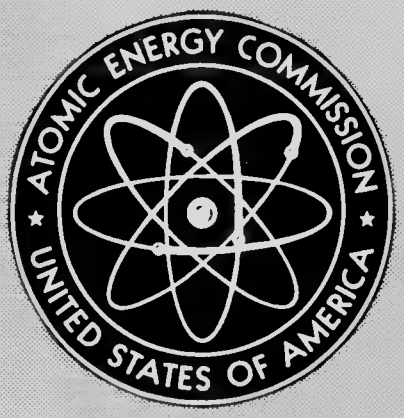

NMI-1239
METALLURGY AND CERAMICS

A METALLOGRAPHIC STUDY OF THE SWELLING OF URANIUM AND URANIUM ALLOYS

By
A. Boltax
A. R. Lumbert
H. M. Green

August 17, 1960

Nuclear Metals, Inc.
Concord, Massachusetts

UNITED STATES ATOMIC ENERGY COMMISSION • OFFICE OF TECHNICAL INFORMATION

USAEC Office of Technical Information Extension
Oak Ridge, Tennessee

NMI-1239

A Metallographic Study of the Swelling of Uranium and Uranium Alloys

by

A. Boltax and A. R. Lumbert
and
H. M. Green

August 17, 1960

Nuclear Metals, Inc.
Concord, Massachusetts

Contract No. AT(30-1)-1565

A. R. Kaufmann
Technical Director

TABLE OF CONTENTS

LIST OF TABLES

LIST OF FIGURES

LIST OF FIGURES (Cont'd.)

LIST OF FIGURES (Cont'd.)

ABSTRACT

The behavior of inert gases were studied in inoculated uranium and uranium alloy (U-1.6, 2.8, and 10 ^{w}/o Mo, U-2 ^{w}/o Zr, U-0.3 Cr - 0.3 Mo, U-1 and 2 ^{w}/o C, and U-3.8 ^{w}/o Si) samples. Helium was injected into metal samples by alpha particle irradiation krypton by glow-discharge techniques. Following gas inoculation, samples were given various isothermal and thermal cycling heat treatments to permit the formation of gas bubbles. The gas bubbles were observed in the light microscope after mechanical polishing and after chemical etching and in the electron microscope after cathodic vacuum etching.

Helium gas bubbles were observed in the cyclotron-irradiated samples following various heat treatments between 475 and 1075^{o}C. The majority of the gas bubbles in any sample, independent of heat treatment, were between 0.05 and 2 microns in diameter (10^{10} to 10^{14} per cc), and accounted for up to 10 percent porosity. Post-irradiation heat treatments above 900^{o}C gave rise to the formation of a small number (about 10^{5} per cc) of large bubbles between 10 and 150 microns in diameter which accounted for porosities up to several hundred percent. The large volume increase caused by the latter bubbles is similar to that observed in metallic reactor fuel elements irradiated at temperatures above 400^{o}C.

Effects of recrystallization and phase transformations on the behavior of the helium gas bubbles were noted. The nucleation and growth characteristics of the small and large bubbles are discussed.

I. INTRODUCTION

The behavior of metallic fuel elements at elevated temperatures and high burn-ups is intimately connected with the distribution of fission products, in particular the gaseous fission products, xenon and krypton. For most uranium-rich metallic fuel materials used in reactors operating above 600°C it is clear that gaseous fission products are directly responsible for volume instability. Recent irradiation data, obtained at operating temperatures between 300 and 700°C, summarized in Fig. 1, provide evidence for volume instability which appears to be related to gaseous fission products.

The purpose of the experimental work described in this report is to study the behavior of artificially introduced rare gas in uranium and uranium alloy samples. Rare gas was inoculated into the metal samples by alpha particle irradiation, resulting in helium atoms being trapped in the fuel material, and by glow-discharge techniques by which krypton was introduced into uranium.

II. PRIOR WORK

Studies of swelling following alpha particle irradiation have been reported for copper,[1] beryllium,[2,3] and aluminum.[4,5] The swelling occurs in a thin layer approximately 1 mil thick which is formed about 5 to 15 mils below the surface of the metal, depending upon the range of the monoenergetic alpha particles. Barnes[1] has recently reviewed the subject of swelling due to helium in metals: first, diffusion of helium and bubble nucleation; second, bubble growth; and third, coalescence of bubbles. Furthermore, the swelling due to small bubbles (below 1 micron radius) can be satisfactorily described by the perfect gas law, with the gas pressure in the bubble given by the surface energy term $\frac{2\gamma}{r}$, where gamma is the surface tension and r the bubble radius.

The glow-discharge technique, in which the ionized rare gas is introduced into a metal sample that is at a temperature of 600 to 800°C, has been successfully applied to the study of diffusion of argon, xenon, and krypton in metals such as silver and uranium by LeClaire and Rowe[6] and Tobin.[7]

Studies of swelling in neutron-irradiated metallic fuels have been recently reviewed by Barnes et al.[8] and Churchman.[9] References to some of these results will appear later in the report.

III. EXPERIMENTAL METHODS

A. Materials Used

The materials used in this investigation are described in Table I.

For the cyclotron irradiation experiments specimens 1 inch by .25 inch by 0.04 inch were obtained from material machined or rolled to a thickness of about 40 mils; those for the glow-discharge experiment were discs 2 inches in diameter by 0.01 inch thick, and hollow cylinders 2 inches OD by 0.01 inch thick by 4 inches long obtained from material machined or rolled to about 10 mils.

Prior to the cyclotron irradiation, most of the uranium and uranium alloy specimens were annealed for two hours at 850°C to put them in a standard starting condition.

B. Cyclotron Irradiation

The alpha particle irradiation was performed in the external position of the 31.5 Mev alpha particle beam of the MIT cyclotron. The external target holder is a water-cooled aluminum block, as described by Ells and Evans.[4] The sample, clamped against a water-cooled aluminum target holder, was probably below 50°C throughout the alpha particle irradiation. The helium concentration in the irradiated samples was calculated from the integrated alpha beam current, the area of the alpha beam, and the thickness of the helium-rich layer. The volume of the helium-rich layer, about one-hundredth of a cubic centimeter, was estimated from metallographic evidence. The units of gas concentration are given in terms of the gas:volume ratio (GVR), which is the volume of gas measured at STP per unit volume of metal. Conversion from integrated beam current to GVR is given by

$$GVR = \frac{I_t K V_o}{V N_o} \qquad \text{Equation 1}$$

where I_t is the integrated alpha beam current in microampere hours, K is the conversion for microampere hours to doubly ionized alpha particles per hour, V_o is the volume of one mole of gas at STP, V is the volume of irradiated material, and N_o is Avagadro's number. A gas concentration of approximately 0.4 GVR per hour can be obtained with an alpha beam current of 10 microamperes. The GVR values reported are probably accurate to + 50 percent.

The penetration of the 31.5 Mev alpha particles into the uranium and uranium alloy samples ranges between 3.5 and 5 mils. A small amount of the alpha particle energy is lost in penetrating an aluminum diaphragm which separates the internal and external chambers (the latter containing helium at one atmosphere) of the cyclotron before penetrating the sample. The majority of the samples studied were irradiated for exposures of 50 microampere hours, which is approximately equivalent to the gas concentration formed at one atomic percent burn-up; that is, the helium concentration in a small region of the sample is equivalent to the concentrations of xenon and krypton that would be present in uranium after one atomic percent burn-up. One series of samples was given a series of interrupted irradiation and annealing treatments. The irradiation schedule used for the latter samples is described in Table II.

Examination of the entire cross-section of the cyclotron-irradiated samples reveals a variation in gas concentration across the width of the sample, because the sample width is greater than the width of the uniform portion of the alpha beam. This result permits a study of the swelling behavior as a function of gas concentration for a particular heat treatment.

C. Inoculation of Inert Gas by Glow-discharge Technique

A schematic diagram of the glow-discharge tube is shown in Fig. 2. The portion of the tube containing the cathode is made of vycor and is approximately 15 inches long. The cathode (approximately 2-3/4 inch diameter) is constructed with a hollow lead to allow a thermocouple to be placed in close proximity to the sample. A stainless-steel sleeve supports the cathode, and is made of the same material as the cathode to eliminate any differences due to thermal expansion. The vycor chimney serves two purposes: first,

it holds the sample in good contact with the cathod; second, it contains the cylindrical sample and confines the glow discharge.

The top section of the tube is made from a standard 3-inch pyrex pipe cap. A glass side arm is used for the vacuum outlet and gas inlet. The anode is made of stainless steel with a shaft that extends approximately one inch into the chimney. "Kovar" seals are used to bring the electrodes out of the chamber. The gasket between the top and bottom portions of the chamber is water cooled.

A block diagram of the remainder of the apparatus is shown in Fig. 3. The rare gas supply passes through a gettering and drying train consisting of zirconium chips followed by Linde molecular sieves. The rare gas supply and the vacuum system are connected to a common manifold. This arrangement affords complete control of pressure within the glow-discharge tube as well as maximum flexibility for operation of additional units. A dynamic reading vacuum gage incorporated directly in the discharge-tube line provides constant monitoring of the pressure.

Removal of extraneous gases was originally accomplished by the liquid nitrogen cold traps, but more complete removal is obtained with a getter tube filled with uranium chips and heated with a split muffle furnace. The gettering tube is attached to the top of the glow-discharge chamber. An external split muffle furnace is used to heat the samples to a maximum temperature of 900°C.

The sample is introduced into the glow-discharge chamber in the form of a thin disc and a cylindrical sheet. Tantalum foil is placed between the cathode and sample, and a tantalum ring between disc and cylindrical sample pieces. This is necessary to prevent bonding of the sample to adjacent pieces. Then the sample is outgassed at a temperature higher than that to be used during the run. When outgassing is completed, the temperature of the sample is dropped to the desired run temperature, and the chamber is then flushed with krypton. The chamber is then re-evacuated and filled with krypton to the desired run pressure. The glow discharge is initiated and the run started.

D. Heat Treatment

Following irradiation the samples were sectioned and the individual sections given various post-irradiation annealing treatments. The details of the heat treatments and their purpose are summarized in Table III. The heat treatments were performed in vycor or quartz capsules containing one atmosphere of helium at temperature. Samples were wrapped in tantalum to prevent reaction with the vycor or quartz container. After the heat treatment the capsules were permitted to cool in air before removal of the specimens.

E. Metallographic Examination

Samples were examined in the light microscope after mechanical polishing and subsequent etching in a solution of 1/3 glacial acetic acid and 2/3 nitric acid, except for the uranium-2 $^{w}/_{o}$ zirconium samples, which were etched in a solution of 10 parts nitric acid, 10 parts sulfuric acid, and 1 part hydrofluoric acid. Preliminary electron microscope studies* were performed on replicas of samples, repolished mechanically following the light microscopy study and then given a cathodic vacuum etch.

IV. RESULTS

A. Cyclotron Irradiation

1. General Results

Metallographic examination of the irradiated samples indicated that either the helium was in solid solution in the uranium or the helium bubbles were too small to be detected with a light microscope. As an example, Fig. 4 is a photomicrograph of an as-irradiated sample of ingot uranium. Following any of the heat treatments described previously in Table III, helium bubbles could be detected in all of the uranium samples.

- - - - - - - - - - - - -

* The electron microscopy was performed by C. L. Angerman, E. I. du Pont de Nemours, Inc.

The bubbles observed fall into one or the other of two classes. Class I bubbles are between 0.05 and 2 microns in diameter with densities varying between 10^{10} and 10^{14} bubbles per cubic centimeter, which can cause up to about 10 percent swelling. The behavior of the Class I bubbles can be approximated by use of the perfect gas law with the pressure given by the term $\frac{2\gamma}{r}$ where γ is the surface tension and r the bubble radius. Class I bubbles were observed in all samples, independent of heat treatment and alloy composition. The size and number of the bubbles are dependent upon the post-irradiation annealing time and temperature and do not appear to be markedly dependent upon the alloy content of the sample.

Class II bubbles are between 10 and 150 microns in diameter with densities of the order of 10^5 bubbles per cubic centimeter, which can account for swellings up to 300 percent. The Class II bubbles were observed only after heat treatments at 900°C or above. All of the materials studied show Class II bubbles after a 90-hour anneal at 1075°C. Class II bubbles do not appear to be created by a process continuous with the formation and growth of Class I bubbles but rather appear to be related to some discontinuous or catastrophic bubble growth mechanism. The size of the Class II bubbles appears to be related to the alloy composition of the sample and, in particular, to the strength of the sample at high temperature.

In the following presentation, the results of metallographic examination of samples after post-irradiation annealing are reported separately for each alloy system. A summary of the available measurements of bubble size and density is given in Table IV for specimens given a 90-hour isothermal post-irradiation annealing treatment.

2. Uranium

a. Dingot Uranium

Examples of the appearance of the helium bubbles formed in dingot uranium following alpha particle irradiation and various post-irradiation annealing treatments are shown in Figs. 5, 6, 7, and 8. In most of the photographs the Class I bubbles cannot be resolved at 1500X. Preliminary electron microscopy studies reveal the small Class I bubbles as shown in Fig. 12.

The chemical etch used in this study reveals the sub-grain boundaries in uranium as they are outlined by impurities. This effect has been described in detail by Robillard.[10] As shown in Figs. 5c and 5d, the sub-grain boundaries are usually not related to the uranium grain boundaries revealed by examination in polarized light. The black boundaries that appear in the helium bubble band, Fig. 5e, are presumed to be sub-boundaries that are decorated with helium bubbles.

The first occurrence of Class II bubbles in the dingot uranium samples is shown in Fig. 5f following a 300-hour heat treatment at 900°C. Three small inclusions that lie within the bubble band are shown in Figs. 5f and 5g but do not appear to be causing any accelerated bubble growth in their vicinity. The 1000-hour post-irradiation annealing heat treatment at 900°C and the 90-hour heat treatment at 975°C give rise to a region free of bubbles in the center of the helium band. This bubble-free region will be noted in other samples of uranium and is related to the presence of Class II bubbles. The mechanism of the formation of this gas-free region at the center of the bubble band will be described later.

A 2-hour anneal at 1075°C was carried out in an attempt to reveal the early stage of formation of Class II bubbles. The photomicrograph in Fig. 6a reveals two large bubbles that appear to be in an early stage of development as compared to the Class II bubbles seen in the other photomicrographs after a 90-hour anneal at 1075°C. Another item of interest shown in Fig. 6c-6e is the variation in bubble size that occurs as a function of helium concentration in the uranium dingot sample. In the high concentration region in the center of the sample (Fig. 6c) the bubbles are approximately 0.7 micron in diameter and increase to a diameter of about 2 microns at a gas composition approximately 1/5 of the concentration in the central region (Fig. 6e). The observed variation in bubble size with concentration is consistent with the concept of higher nucleation rates with higher supersaturation levels.

The behavior of helium bubbles in dingot uranium that was irradiated in a cold-worked condition is shown in Figs. 7 and 8 The rolled sample, after the 90-hour post-irradiation anneal at 600°C (Fig. 7a), shows a closely spaced network of sub-boundaries in the helium gas band The

network is presumed to be the remains of incomplete recrystallization, delayed by pinning of the sub-boundaries by the small helium bubbles. A similar effect of gas bubble pinning of grain boundaries has been reported by Ells and Evans. After the 90-hour post-irradiation anneal at 730°C the difference in appearance between the previously cold-worked material and the annealed material is slight, with the worked material appearing somewhat more disturbed as evidenced by the greater density of sub-boundaries. The 90-hour anneal at 900°C produces a small number of Class II bubbles in the previously worked dingot uranium sample and a bubble-free region at the center of the gas band (Fig. 7d). Further increases in post-irradiation annealing time and temperature cause increases in the number of Class II bubbles, and an increase in size and decrease in the density of the Class I bubbles. After a 90-hour post-irradiation anneal at 1075°C (Fig. 8f), there was only a very small, if any, bubble-free region in the center of the bubble band.

The effect of the various thermal cycling treatments on the appearance of the helium bubbles is shown in Fig. 9. Except for the bubbles formed during the alpha-beta thermal cycle the helium bubbles are too small to be resolved by the light microscope. The 100 alpha-beta thermal cycles (Figs. 9b and 9c) give rise to about 0.2×10^{12} bubbles per cubic centimeter of .4 micron average diameter. These bubbles can account for a volume change of about 7 percent. A calculation of the gas concentration yields a value of 2.5 GVR if it assumed that surface tension of uranium is taken as 1,000 dyne-centimeters. This value of gas concentration is in agreement with the nominal gas concentration of 4 GVR calculated from the integrated alpha beam current. Note also that the alpha-beta thermal cycle produces severe distortion of the sample and the bubble band.

Examples of the behavior of helium in dingot uranium after combined thermal cycling and isothermal heat treatment are shown in Fig. 10. Comparison of these photographs with those obtained on samples given either a similar isothermal or thermal cycling heat treatment indicates that the combined heat treatments do not cause unusual swelling. Figs. 10b and 10c show further indications of the early formation of Class II bubbles.

b. Ingot Uranium

The behavior of helium in ingot uranium is similar in many respects to that reported above for dingot uranium. The principal difference between the two types of uranium is that Class II bubbles are observed after annealing at lower temperatures in the dingot uranium than in the ingot uranium. The series of photographs shown in Figs. 11, 12, 13, and 14 illustrate the appearance of helium bubbles after various post-irradiation annealing heat treatments.

Fig. 11b shows the microstructure of an ingot uranium sample that has been heavily etched in the nitric-glacial acetic acid etchant. The heavy etching reveals the sub-boundaries (thin black lines) and traces of the gamma boundaries (coarse white bands). The interpretation of structures similar to these has been described by Robillard, as mentioned previously. The thin black lines revealed in Fig. 11c were originally thought to be fine microcracks, but further analysis revealed that they were probably decorated sub-boundaries. It is interesting to note that sub-boundaries are not revealed by the cathodic vacuum etch used in the preparation of the replicas for the electron microscopy studies.

Fig. 12 shows the appearance of the helium bubbles formed in ingot and dingot uranium samples following a 90-hour post-irradiation anneal at 900°C. The bubble size and density are essentially identical; however, one difference in the appearance of the bubbles should be noted. The submicron bubbles in the ingot uranium sample are for the most part isolated from one another whereas in the dingot uranium sample there are numerous occurrences of overlapping bubbles and in several places long strings of bubbles may be seen. This tendency toward overlapping of bubbles in dingot uranium on the submicron scale is further demonstrated on a micron scale in Fig. 6 in the sample annealed for 90 hours at 1075°C.

Fig. 13c illustrates the bulging of the surface of the sample above the Class II bubbles. This localized bulging or swelling of the sample is an indication that some of the bubbles are growing by mechanical deformation of the surrounding metal. Lack of localized swelling of the sample would be an indication that the bubble growth was primarily by vacancy flow. This latter form of behavior was illustrated in a rolled dingot

uranium sample annealed for 90 hours at 975°C, as shown in Figs. 8c and 8d. Notice also that when vacancy flow is the predominant mechanism for growth of Class II bubbles a bubble-free region in the center of the helium bubble band is formed.

The behavior of helium in the thermally cycled ingot uranium samples, Fig. 15, is similar to that reported for the dingot uranium sample except that in the ingot uranium sample the alpha-beta cycle does not give rise to bubbles that can be resolved in the light microscope.

Preliminary studies of the combined isothermal and thermal cycling heat treatments do not reveal any anomalous swelling, as indicated in Fig. 16. In a similar manner metallographic evidence indicates that the samples given the interrupted cyclotron-irradiation and heat treatment cycle do not show any signs of anomalous swelling, as shown in Fig. 17. The thin black lines diagonal to the bubble band in Fig. 17c do not appear to be sub-boundaries and may be evidence of microcracks; however, further evidence is needed before the presence of microcracks can be substantiated.

c. Arc Melted Ingot Uranium

Limited studies of the behavior of helium in arc melted ingot uranium indicate similar results to that reported for worked and annealed ingot uranium. The results obtained are summarized in Fig. 18. The as-cast material contains uranium carbide in a dendritic form. Annealing at 900°C and higher tends to alter the appearance of the uranium carbide dendrites. The results indicate that the uranium carbide particles do not enhance the nucleation of Class II bubbles.

d. High Purity Uranium

The limited studies of the behavior of helium in high purity uranium do not permit a detailed comparison of this material with the other materials previously reported. However, two results of interest were obtained and will be described. Fig. 19 shows the helium bubble band in a high purity uranium sample after a 90-hour post-irradiation anneal at 900°C. The appearance of the band is similar to that observed in dingot and ingot samples given the identical heat treatment. Preliminary experiments

with combined isothermal and thermal cycling heat treatments indicate that Class II bubbles will form in this material, as illustrated in Fig. 20. This result indicates that the nucleation sites for Class II bubbles may be related to trace impurity elements and not to the major impurities in uranium.

3. Uranium Carbon Alloys

Helium bubbles formed during post-irradiation heat treatment in the uranium-1 and -2 $^{w}/o$ carbon alloys[11] are shown in Fig. 21. In general the behavior ofthese alloys is similar to that indicated by the results obtained on ingot uranium. Apparently the uranium carbide dispersion does not give rise to any anomalous swelling. It is not clear whether the presence of the uranium carbide particles affects the size of either the Class I or Class II bubbles observed.

4. Uranium Molybdenum Alloys

a. Uranium - 1.6 $^{w}/o$ Molybdenum

Figs. 22 and 23 illustrate the behavior of helium in uranium - 1.6 $^{w}/o$ molybdenum alloy samples following various isothermal and thermal cycling heat treatments. Since 1.6 $^{w}/o$ molybdenum is insufficient to completely retain the gamma phase on cooling, the transformation of gamma uranium to alpha plus epsilon is evident in all the microstructures. The variations in the appearance of the transformation product are a result of the transformation characteristics of the alloy.

The Class I helium bubbles formed in the dilute uranium-molybdenum alloys after the various post-irradiation annealing treatments could not be resolved with the light microscope. As shown in Fig. 22, the evidence for the bubble band is mainly a thin band of transformed material which has a somewhat different appearance from the remainder of the sample. Fig.22e shows that the portion of the sample through which the energetic alpha particles have passed did not appear to transform during the post-irradiation heat treatment. It is unlikely that this is the result of atomic displacement effects due to the alpha particles; rather, it may be due to the slightly different etching behavior of this material compared to the remainder of the sample. The etching times for these samples were very

short (the order of five to fifteen seconds) and the bulk of the sample may have etched before the material near the irradiated surface.

The thermal cycled uranium - 1.6 ^{w}/o molybdenum sample shows an interesting interaction between the transformation products and the helium bubble band.* As noted in Fig. 23, the transformation products do not appear within the confines of the bubble band. Apparently, the helium bubbles were effective in preventing the transformation from occurring within the gas-containing regions. The effects of Class I bubbles on phase transformations will be discussed further in Section 4c below.

b. Uranium - 2.75 ^{w}/o Molybdenum

The appearance of the helium bubbles in uranium - 2.75 ^{w}/o molybdenum samples following various post-irradiation annealing heat treatments is shown in Fig. 24. With the exception of the sample given isothermal heat treatment at 600^{o}C, which permitted the eutectoid decomposition of the gamma phase, the samples retained the gamma phase following post-irradiation heat treatment, except in the region containing helium. Apparently, the decomposition of the gamma phase occurred only in the region of the sample containing the helium bubbles. A possible explanation of this effect may be that the helium bubbles act as nucleation sites for the decomposition of the gamma phase, which in the absence of these sites can be retained as a metastable phase under the heat treatment conditions studied. Note that Class II bubbles are not observed in the uranium - 2.75 ^{w}/o molybdenum until the sample is heat treated at 1075^{o}C.

---

* The alpha-beta thermal cycling treatment used for the dilute U - Mo alloys, namely, 1.5 hours at 600^{o}C followed by 10.5 hours at 715^{o}C, was suggested by W. McDonell of E. I. du Pont de Nemours, Inc. McDonell has found that the high temperature transformation in the U - Mo alloys is sluggish as compared to the low temperature transformation; therefore, a longer time was used to permit the high temperature reaction.

c. Uranium - 10 $^{w}/_{o}$ Molybdenum

The metallographic appearance of helium bubbles in uranium - 10 $^{w}/_{o}$ molybdenum samples following various isothermal and thermal cycle post-irradiation annealing heat treatments is shown in Figs. 25, 26, and 27. The uranium-molybdenum samples were irradiated in two pre-irradiation conditions, (1) retained gamma phase, and (2) transformed by a pre-irradiation heat treatment of 48 hours at 550°C. The results indicated that the pre-irradiation condition of the alloy had little effect on the behavior of the helium bubbles.

For the most part Class II bubbles are not observed in the uranium - 10 $^{w}/_{o}$ molybdenum alloy samples until the post-irradiation heat treatment is performed at 1075°C. There are, however, some limited indications of Class II bubbles after a 90-hour isothermal anneal at 975°C. Figs. 26 and 27 show that the thermal cycling heat treatments or combined thermal cycling and isothermal post-irradiation heat treatments studied do not lead to any excessive swelling. The photomicrographs do show, however, two interesting interactions between the helium bubbles and the transformation products. In Figs. 26a and 26b it is apparent that the gamma phase did not transform within the region of the sample containing the helium bubbles. This phenomenon is similar to that described previously for the uranium - 1.6 $^{w}/_{o}$ molybdenum alloy. Fig. 26c shows that in a region of the sample where gas concentration is low (near the edge of the sample) the transformation was able to proceed across the low-concentration helium gas region and did not appear to lead to any noticeable effect on the helium bubbles. In Fig. 26b the major portion of the sample is partially transformed, whereas the region of the sample containing the helium gas is almost totally transformed. It is suggested that the alpha plus epsilon phases formed at 475°C did not return to the gamma phase during the heat treatment at 800°C due to the effects of the Class I helium bubbles on the high temperature phase reversion.

The photomicrographs in Fig. 27 reveal that combined isothermal and thermal cycling heat treatments do not give rise to any excessive growth of the helium bubbles.

d. Uranium 0.3 ^{w}/o Molybdenum - 0.3 ^{w}/o Chromium

The uranium - 0.3 ^{w}/o molybdenum - 0.3 ^{w}/o chromium alloy was developed at Nuclear Metals, Inc.[12] as an alloy that would be capable of retaining the beta phase on cooling to room temperature. The results of the metallographic study of helium bubbles formed in this alloy during the post-irradiation annealing heat treatment are shown in Figs. 28 and 29. The extent of the swelling noted is similar to that observed in the uranium ingot material. The cracks visible in the samples were produced as a result of the pre-irradiation heat treatment, which consisted of a one-hour anneal at 800°C followed by an oil quench. Fig. 29 shows an interesting phenomenon where one of the cracks passes through the helium bubble region. In this region it appears that the crack may be the site of a Class II bubble.

e. Uranium - 3.8 ^{w}/o Silicon

Limited studies of the behavior of helium in uranium - 3.8 ^{w}/o silicon alloys indicate that the Class II bubbles can be formed during long time heat treatment at 900°C. Fig. 30 shows evidence of Class II bubbles in uranium - 3.8 ^{w}/o silicon alloys heat treated at 900 and 975°C.

B. Glow-discharge Experiments

A complete summary of the glow-discharge runs is shown in Table V. The samples in these runs were either copper or uranium or a combination of uranium and copper. The temperature of the runs varied from 550 to 785°C, and the power output ranged from .33 to 9.8 kilowatt hours.

1. Results of Gas Analyses

Analysis for krypton gas was carried out on various sections of the glow-discharge samples to determine the amount of gas present and the quantity at specific locations.

In order to make the determination the samples were sectioned at various locations (see Figs. 31, 32, and 33) and melted separately in a vacuum-fusion furnace. The gas released from the melt was collected in

a bottle for analysis in a mass spectrograph. The quantity of krypton gas, determined by comparison with a krypton gas standard, was used to determine the moles of krypton contained in the sample.

Metallographic studies indicate that the gas was contained in a 1-mil surface layer. The gas concentration in the surface is expressed in terms of GVR, which is the ratio of gas volume measured at standard temperature and pressure to the volume of metal containing the gas. Since one $^{a}/_{o}$ burn-up of uranium gives rise to 4.7 GVR of krypton or xenon, a GVR of 1.0 is equivalent to the gas present at approximately .21 $^{a}/_{o}$ burn-up. A summary of the gas analysis for the sectioned glow discharge samples is given in Table VI.

2. Additional Observations

In observing the glow-discharge cylindrical specimens it was noted that bands of etched and deposited material formed circumferentially at different heights. Two examples are shown in Figures 32 and 33. In both figures the darkest band appears at the bottom of the photograph. This was the portion nearest the disc during the glow discharge. The material from this end of the specimen contained the largest percentage of krypton gas. The copper specimen in Figure 32 contained many bubbles on its surface and, coincident with this, sections taken from this contained the largest volume of gas (see Table VI). The uranium specimen in Figure 33 shows the typical banding that occurs, and the dark line halfway up the photograph shows where the top of the glow was during the run. The surface of the uranium sample has the appearance of an oxide film, as did the copper specimens. The bright etched appearance of the copper sample shown in Fig. 32 is unusual in this respect.

Observations of the glow-discharge specimens following run GD-5 (uranium disc and copper cylinder) revealed that uranium had deposited onto the copper cylinder. There was no evidence of copper on the uranium disc.

Metallographic examination of samples of uranium from glow-discharge run No. 9 and copper from glow-discharge run No. 7 was performed. Examples of the results obtained are shown in Figs. 34 and 35. In the case of the uranium samples, a 90-hour post glow-discharge anneal at 900°C was not sufficient to reveal the presence of krypton bubbles with the light

microscope. However, the copper samples do show krypton bubbles near the surface of the samples, (see Fig. 35), following a 90-hour heat treatment at 900°C and 975°C. Preliminary observations indicate the presence of both Class I and Class II bubbles in the copper glow-discharge samples. Additional studies are planned for the uranium and copper glow-discharge samples.

V. DISCUSSION AND CONCLUSIONS

A. Cyclotron Irradiation

1. General Discussion

As mentioned previously, all of the observations of the helium bubbles can be reduced to a consideration of two different classes of helium bubbles: Class I bubbles, which are micron size and smaller, and Class II bubbles, which range from 10 to 100 microns in diameter. The behavior of Class I bubbles in uranium and uranium alloys is typical of that of the helium bubbles formed in cyclotron-irradiated and annealed aluminum, beryllium, and copper. Because of the high density of these bubbles (10^{14} bubbles per cc.) it is likely that homogeneous nucleation takes place and that prolonged heat treatment results in the growth of the bubbles by a coalescence process, i.e., the re-solution of the smaller bubbles and growth of the larger bubbles. A theory of coalescence has been described by Boltax.[5]

With the limited resolution of the light microscope it was not apparent in most cases that complex heat treatments, which cause boundaries to move through the helium bubble region, gave rise to any excessive swelling. One notable exception is the behavior of the helium bubbles in dingot uranium following 100 thermal cycles between 600°C and 730°C. The results, as shown in Fig. 9c, reveal bubbles of approximately 0.4 microns in diameter, which are significantly larger than those formed in dingot uranium samples annealed for 90 hours at either 600° or 730°C, and larger than those formed by a 90-hour post-irradiation anneal at 900°C. This result suggests that swelling may be enhanced by thermal cycling as compared to isothermal heat treatment at either of the extremes of the thermal cycle. However, the results on ingot uranium do not indicate this same effect.

Since the size and density of Class I bubbles seem to be independent of the alloy content of uranium base materials, and since this class of bubbles does not account for a very large amount of swelling, it would appear advisable to concentrate attention on the Class II bubbles. The size of Class II bubbles appears to vary with alloy content and they account for a large amount of swelling. A limited amount of qualitative data on the diameter of helium bubbles as a function of post-irradiation annealing temperature for a constant time is summarized in Fig. 36. The results indicate the discontinuous characteristic of the Class II bubbles.

A plot of the bubble diameter versus the reciprocal of the absolute temperature at which the specimen was annealed should, if the process is diffusion controlled, obey the relationship

$$d = K_e^{-Q/RT} \qquad \text{Equation 2}$$

where d is the bubble diameter (microns), K is a constant involving some function of time, Q is the activation energy for bubble growth (calories per mole), R is the gas constant and T is the temperature (^{o}K). From the limited data on Class I bubble diameter as a function of post-irradiation annealing temperature the activation energy of bubble growth was determined to be of the order of 45,000 cal/mole. This result may be compared with the value of 11,000 cal/mole for aluminum[5] and 40,000 cal/mole for the swelling of beryllium.[2]

The order of magnitude agreement of the number of Class II bubbles per cubic centimeter in all of the uranium base alloys studied indicates that the number of nucleation sites for Class II bubbles is not related to the alloy content of the material but to some uniform characteristic of all the alloys, such as the level of some impurity element. The observations made on the size and occurrence of Class II bubbles appear to be consistent with the concept of nucleation of Class II bubbles on particular, but as yet unspecified types of inclusions. One suggestion of such a mechanism is described in detail in the following paragraphs.

During post-irradiation annealing of cyclotron-irradiated samples at temperatures below 900^{o}C, the nucleation sites for Class II bubbles appear

to be ineffective. However, post-irradiation heat treatment at higher temperatures gives rise to Class II bubbles within the helium band. It is therefore suggested that the inclusions which nucleate Class II bubbles undergo some sort of transformation or decomposition at high temperatures which makes them capable of nucleating Class II bubbles. In the experiments described, this decomposition or transformation would be expected to occur at about 900°C and above. It is conceivable that under neutron irradiation these inclusions may be capable of nucleating Class II bubbles at lower temperatures and account for the large swellings observed during neutron irradiation.

Fig. 37 shows a schematic diagram of the appearance of the helium bubbles around an inclusion which can nucleate Class II bubbles at high temperatures. Following decomposition, transformation, or loss of coherency of the particle with the matrix, the gas in the Class I bubbles at the surface of the particle forms a continuous envelope that is no longer restrained by surface tension but by the mechanical strength of the matrix. At high temperatures the mechanical restraint is not sufficient to prevent rapid growth of the bubble. Bubble growth may become catastrophic as the bubble begins to overlap numerous small bubbles of considerably higher pressure. The suggestion of catastrophic growth is made because of the lack of observation of the development of Class II bubbles from Class I bubbles. In only a few cases is there evidence for the appearance of Class II bubbles in what might be taken to be their initial stages of formation or development. Examples of such evidence were obtained by short time annealing at 1075°C and are shown in the photomicrographs in Figures 6a and 13b. The appearance of the early stages of these Class II bubbles is consistent with the hypothetical mechanism described in Fig. 37. Further work will be required to identify the nucleation sites for Class II bubbles.

2. Role of Vacancies in Swelling

The importance of vacancies in swelling of metals has been discussed by Barnes. He has considered in some detail the sources of vacancies in metals and has concluded that surfaces, grain boundaries and isolated point sources are the major contributors of vacancies to the

system. During the rapid growth of gas bubbles, vacancies (or free space) can be supplied to bubbles by either of two general processes: diffusion of vacancies into the bubbles or plastic deformation by creep of the matrix material surrounding the bubble. If vacancy accumulation occurs by the latter means, then there should be some evidence of the deformation, such as a bumping of the surface or distortion of the material in the vicinity of large bubbles.

An example of bubble growth by plastic deformation is shown in Fig. 13c. An example of swelling where vacancy diffusion was probably the major factor in the bubble growth is shown in Fig. 8c. In this latter photomicrograph there is little evidence of distortion of the surface in the vicinity of the Class II bubbles. High magnification photographs reveal the presence of a bubble-free region of metal in the center of the helium bubble band. The size of this gas-free region appears to vary along the width of the sample, becoming narrower as the gas concentration and the concentration of Class II bubbles decreases. It is suggested that bulk flow has occurred in the center of the bubble band due to a form of Kirkendall-effect. The accumulation of vacancies in the Class II bubbles is balanced by the flow of uranium atoms from around the gas bubbles to the center of the bubble band. This diffusion process probably occurs along the sub-grain or grain boundary which passes through the center of the bubble band and which is revealed by a decoration of small bubbles.

The Class I bubbles in the bulk of the helium band act as inert markers and thus permit an estimate of the amount of bulk flow which has occurred. The conditions necessary for bulk flow are that, first, Class II bubbles must be formed, and second, the Class II bubbles must grow principally by vacancy diffusion rather than by plastic deformation. All of the photographs that show bulk flow are consistent with these two conditions.

3. Swelling Resistance of Cyclotron-Irradiated Materials

Since the size and density of Class I bubbles were similar in all of the uranium-base samples examined, an evaluation of the swelling resistance of a given material involves consideration of the temperature at which Class II bubbles were first noted and the size of the Class II

bubbles. Table VII gives a relative listing of swelling behavior in order of decreasing swelling resistance. For comparison, the swelling resistance of fissionable materials under neutron irradiation is also given in Table VII. It is readily apparent that the swelling behavior of cyclotron-irradiated materials does not show a one-to-one correspondence with the swelling behavior of neutron-irradiated materials.

The swelling resistance of cyclotron-irradiated materials generally increases with increasing strength of the material, with the possible exceptions of uranium - 1.6 ^{w}/o molybdenum and uranium - 3.9 ^{w}/o silicon, whereas the order of increasing swelling resistance for neutron-irradiated material shows no general trend with alloy content or alloy strength. The lack of correspondence between the swelling behavior of cyclotron-irradiated and neutron-irradiated materials does not mean that the results obtained in cyclotron irradiation experiments are not of significant value, but rather it demonstrates the complexity of the swelling phenomena. It further suggests that a detailed comparison of swelling in cyclotron- and neutron-irradiated materials will lead to a greater understanding of the behavior of rare gasses in fissionable metals.

4. Interactions Between Gas Bubbles and Transformation Products

Although there is little evidence of the effect of phase transformations, recrystallization and thermally-induced phase reversal on the nucleation and growth of helium bubbles in uranium-base alloys, there is considerable information on the effects of helium bubbles on phase transformations and the distribution or configuration of the transformation products. In several of the uranium - molybdenum alloys there is evidence for both inhibition and acceleration of phase transformations in the region containing the helium gas bubbles. This dual influence of gas bubbles is further evidence for the complex behavior of rare gases in metal alloy systems. In the examples noted there is evidence that Class I bubbles can inhibit transformation by pinning boundaries and, also, evidence of helium bubbles providing nucleation sites for the transformation or decomposition of a metastable phase. Such interactions between the transformation reactions of the alloys and the fission gas

bubbles in neutron-irradiated materials may be important in determining the swelling behavior of uranium alloys. For example, an analysis of phase reversal phenomena in uranium - 10 ^{w}/o molybdenum or 10 ^{w}/o niobium on the basis of thermal decomposition in the absence of Class I bubbles may be inadequate to explain the thermal decomposition rates in the presence of Class I bubbles.

One further suggestion is offered regarding the phase reversal mechanism and its relationship to the anomalous swelling behavior of uranium - molybdenum or uranium - niobium alloys. The results of the present investigation did not show any accelerated swelling under the influence of thermally-induced phase reversal. Furthermore, the results obtained indicate that moving phase or grain boundaries do not appear to cause any accelerated swelling. It is therefore suggested that a possible mechanism for anomalous swelling in alloys that show irradiation-induced phase reversal is related to the effect of phase reversal phenomena on the behavior of nucleation sites for Class II bubbles. For example, phase reversal in the vicinity of an inclusion may give rise to a loss of coherency due to the local stresses generated by the phase transformation. The loss of coherency between the inclusion and the matrix may give rise to the catastrophic form of swelling associated with Class II bubbles at an earlier stage or lower temperature than that which would occur in the same material if the phase reversal mechanism were absent. Thus, it is suggested that phase reversal may not act directly as the mechanism for accelerated swelling but rather that it affects the nucleation sites for Class II bubbles, which in turn determine the swelling behavior of fissionable material.

B. Glow-discharge Experiments

The results obtained indicate that the glow-discharge technique is capable of introducing reasonably high concentrations of krypton into uranium and copper. Preliminary metallographic studies of the glow-discharge samples show indications of krypton bubbles in the copper samples but reveal a lack of evidence of krypton bubbles in uranium. Further studies of the size and density of the krypton bubbles in both copper and uranium are

planned. It is expected that a comparison of the behavior of krypton and helium in copper (the later results reported by Barnes) will show whether there is a large difference in behavior between the two gases in a given metal. It is hoped that a similar comparison of helium and krypton in uranium will be made in the near future.

VI. TABLES AND FIGURES

TABLE I

Tabulation of Materials Used in Swelling Experiments

Material*	Fabrication History
Uranium, ingot	Cast, extruded, and rolled
Uranium, ingot	Arc
Uranium, dingot	Cast, extruded, and rolled
Uranium, high purity	Cast
U-1.6 Mo U-2.75 Mo U-10 Mo U-0.3 Mo-0.3 Cr U-2 Zr	Cast, extruded, and rolled
U-1 C U-2 C	Arc melted
U_3Si	Cast and extruded
Al-35 U	Cast and extruded
Th, reactor grade "Davidow"	Cast, extruded, and rolled
Cu (tough pitch)	Annealed

* Composition of alloys given in weight percent.

TABLE II

Summary of Interrupted Irradiation and Annealing Equipment *

Run No.	Irradiation Schedule (microampere hours)	
	Group 1	Group 2
1	7	1
2	7 S**	2
3	7	8 S
4	7 S	4
5	10 S	10 S
6***	12 S	25 S

* Each group consists of four ingot uranium samples A, B, C, and D. The heat treatments for the samples after each irradiation are given below:

A = 16 hours at 900°C

B = 16 hours at 550°C

C = 10 thermal cycles 550°C (1 hr); 25°C, 20 mins.

D = 10 thermal cycles 730°C (1 hr); 600°C (1 hr)

** S = Section of sample prepared for metallographic analysis.

*** Run No. 6 is still in progress.

TABLE III

Summary of Post-Irradiation Annealing Treatments

(For uranium and uranium alloys after alpha-particle irradiation)

Heat Treatment			Purpose
	Temp. (°C)	Time (hrs)	
Isothermal	600 730 900 975 1075	90 90 90, 300, 1000 90 2, 90	To study the kinetics of helium gas bubble nucleation, growth, and coalescence.
Thermal Cycling	550 20	1 0.3	Alpha Thermal Cycle - to study the effect of internal stresses due to anisotropic thermal expansion on bubble nucleation, growth, and coalescence.
	A. 730 600 B. 715 600	1 1 10.5 1.5	Alpha-Beta Thermal Cycle - to study the effect of phase transformations on bubble nucleation, growth, and coalescence.
	800 475	1 47	Alpha-Gamma Thermal Cycle - Same as above, except long time at 475°C is necessary to permit decomposition of the gamma phase in U-10 w/o Mo alloys.
Combined Isothermal and Thermal Cycling	900 550 20	90 1 0.3	To study the effect of thermal cycling on the growth of bubbles that were formed by annealing at high temperatures.
	900 730 600	90 1 1	To study the effect of phase transformation on the growth of bubbles that were formed by annealing at high temperatures.
	(Thermal cycling) 900 1000	 4 4	To study the effect of a high temperature anneal on the growth of bubbles that were formed by thermal cycling treatments at lower temperatures.

Table IV

Summary of Measurements of Bubble Diameter in Uranium-Base Alloys Following Cyclotron-Irradiation and Post-Irradiation Annealing Treatments

Material*	Prior Condition	Approximate Bubble Diameters** (microns) After 90-hr Post-Irradiation Anneals At: 600°C	730°C	900°C	975°C	1075°C
U ingot	As rolled	<1	<1		<1 (1,m)	--
	2 hr at 850°C	<1	--	Av = 0.07	0.1-0.5 (1,m)	0.3-1 (100,m)
	Arc melted	--	<1	<1	<1	Av = 1 (80,m)
U dingot	As rolled	<1	<1	<1 (60,f)	Av = 0.5 (100,m)	Av = 0.7 (100,m)
	2 hr at 850°C	<1	<1	Av = 0.07	Av = 0.2 (80,m)	0.7-2 (100,m)
U, high purity	Cast	--	--	<1	--	<1 (100,m)
U-1.6 Mo	2 hr at 850°C	<1	<1	<1	<1 (40,m)	<1 (60,m)
U-2.75 Mo	2 hr at 850°C	<1	<1	<1	<1	--
U-10 Mo	2 hr at 850°C	<1	--	<1	<1 (10,f)	<1 (25,m)
	48 hr at 550°C	<1	<1	<1	<1 (10,f)	--
U-0.3 Mo-0.3 Cr	1 hr at 800°C, O.Q.	<1	<1	<1	<1	--
U-2 Zr	2 hr at 850°C	<1	--	<1	--	0.3-1 (60,m)
U-1 C	Arc melted	--	<1	<1	<1	--
U-2 C	Arc melted	--	<1	<1	<1	--
U-3.9 Si	As cast	--	--	--	<1 (70,m)	--
	Epsilonized	--	--	--	--	--

*Alloy composition given in weight percent.

**Diameters given are for Class I bubbles. Data in parentheses are for Class II bubbles with indication of number: f = few and m = many.

TABLE V

Summary of Glow-discharge Experiments (Krypton Gas)

Run	Voltage Across Tube (volts)	Current Through Tube (ma)	Temp. (°C)	Krypton Pressure (mm-Hg)			Total Power Input (kwh)	Cathode Sample	Remarks
				Start	Min.	End			
GD-4*	625	52	800	3.5	-	3.5	7.50	U cylinder U disc	Pressure maintained
GD-5	625	75	600	2.7	0.7	0.7	.34	Cu cylinder U disc	Pressure not maintained
GD-6	770	70	593	1.6	1.4	1.4	2.39	Cu cylinder Cu disc	Outgassed 36 hours at 800°C
GD-7	770	73	625	1.6	.8	3.2	6.33	Cu cylinder Cu disc	Outgassed 1-1/2 hours at 800°C
GD-8	480	66	560	2.7	2.4	3.1	2.94	U cylinder U disc	Outgassed 1-1/2 hours at 800°C
GD-9	370	68	600	2.4	2.4	2.4	3.02	U cylinder U disc	Outgassed 2 hours at 800°C
GD-10	375	70	600	2.4	.4	2.9	8.10	U cylinder U disc	Outgassed 2 hours at 800°C
GD-11	450	70	785	2.9	2.4	3.1	9.85	U cylinder U disc	Outgassed 1-1/2 hours at 870°C

* Runs 1 through 3 were trial runs

TABLE VI

Summary of Gas Analyses and Calculations of GVR's

Sample	Temp. of Run (°C)	Total Power of Run	Cathode Material	Position*	Weight (gms)	Area (cm^2)	Total Atoms of Krypton ($\times 10^{14}$)	GVR in 2-mil Surface Layer
GD-4	780	7.50	U	A	.601	2.62	21000	6.4***
GD-4-1	780	7.50	U	B	1.089	5.35	Trace	--
GD-4-4	780	7.50	U	F	2.102	1.61	Trace	--
GD-4-5	780	7.50	U	E	4.115	3.09	Trace	--
GD-5	600	.33	Cu	A	5.137	9.86	2100	.17
GD-5-1	600	.33	Cu	B	3.252	3.252	2630	.33
GD-5-2	600	.33	Cu	C	3.269	3.269	350	.044
GD-5-3B	600	.33	Cu	B	3.252	6.45	2270	.283
GD-6	600	2.39	Cu	A	5.168	9.86	470	.037
GD-6-1	600	2.39	Cu	B	3.463	9.80	Trace	--
GD-7	625	6.33	Cu	A	4.691	7.10	26200	2.2
GD-7-1	625	6.33	Cu	B	4.807	9.80	28900	2.30
GD-7-2	625	6.33	Cu	E	1.618	3.49	10200	2.33
GD-8	550	2.94	U	A	4.198	9.06	5500	.50
GD-8-1	550	2.94	U	C	2.611	6.45	30	.0037
GD-8-2	550	2.94	U	E	3.072	1.94	Trace	--
GD-8-3	550	2.94	U	F	3.488	2.45	Trace	--
GD-8-4	550	2.94	U	B	1.172	2.90	110	.031
GD-9-1	600	3.02	U	C	2.160	6.45	Trace	--
GD-9-2	600	3.02	U	D	2.157	7.10	Trace	--
GD-9-3	600	3.02	U	E	2.966	2.26	Trace	--
GD-9-4	600	3.02	U	F	2.768	3.03	Trace	--
GD-9-5	600	3.02	U	C	.818	3.03	Trace	--
GD-9-6**	600	3.02	U	B	1.840	5.65	260	.25
GD-10-1	600	8.10	U	B	3.412	8.06	470	.047
GD-10-2	600	8.10	U	C	3.190	7.10	350	.038

(Table VI continued on the next page)

TABLE VI (Continued)

Sample	Temp. of Run (^{o}C)	Total Power of Run	Cathode Material	Position	Weight (gms)	Area (cm^2)	Total Atoms of Krypton ($\times 10^{14}$)	GVR in 2-mil Surface Layer
GD-11-1	785	9.85	U	B	2.853	8.70	2540	.236
GD-11-2	785	9.85	U	C	2.990	7.74	490	.053
GD-11-3**	785	9.85	U	B	2.732	7.74	1140	.118
GD-11-4**	785	9.85	U	C	2.645	7.74	550	.056

* See Figure 31

** Melted in copper

*** Gas content is not consistent with results obtained on other sections of the specimen. Results were therefore deemed unreliable.

TABLE VII

Swelling Behavior of Fissionable Material In

Order of Decreasing Swelling Resistance

Cyclotron Irradiation	Neutron Irradiation[1]
U-10 w/o Mo	Th-11 w/o U
U-2.75 w/o Mo U-2 w/o Zr	U-10 w/o Mo
U ingot (rolled, annealed, arc melted)	U arc melted (British results)
U high purity	U cast and beta treated
U-1 and 2 w/o C (arc melted)	U-1.5 w/o Mo U-1.6 w/o Zr cast (high Bu rate)
U-1.6 w/o Mo	U rolled and beta treated
U dingot (rolled or annealed)	U-1.2 w/o Mo powder compacts U_3Si
U_3Si (cast or epsilonized)	U-2 w/o Zr cast (low BU rate)
Th (very impure)	U powder compacts
	U-9-12 w/o Nb

Index	Source	Specimen	Burnup Range (^{a}/o)	Temp. Plotted
1	AI	0.38-0.75" dia. rods	0.03-0.7	Av metal temp.
2	WAPD	Two 44-mil clad plates	up to 0.7	Reported temp.
3	ANL	0.2-0.38" dia. rods	0.1-0.7	Av metal temp.
		0.125" dia. rods	0.2-5.3	Av metal temp.
4	APDA	0.1" dia. rods	0.4-2.7	Av metal temp.
5	KAPL	~0.1" dia. oval rods	0.1-3.2	Initial central metal temp.
6	UK	Pellets or cylinders	0.1-0.4	Reported temp.

Fig. 1 - Summary of swelling data for neutron-irradiated fuels. Drawing No. RA-1722

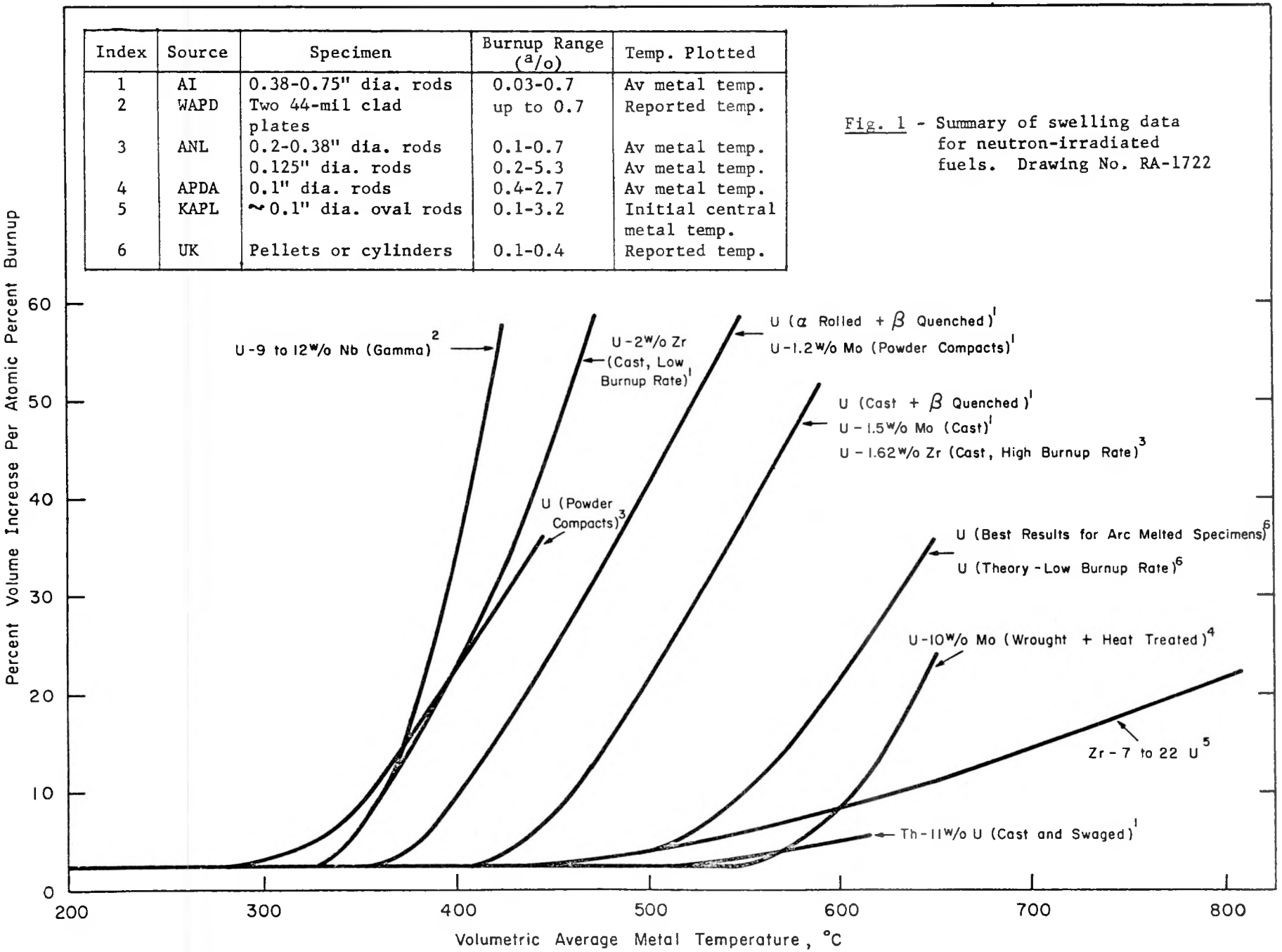

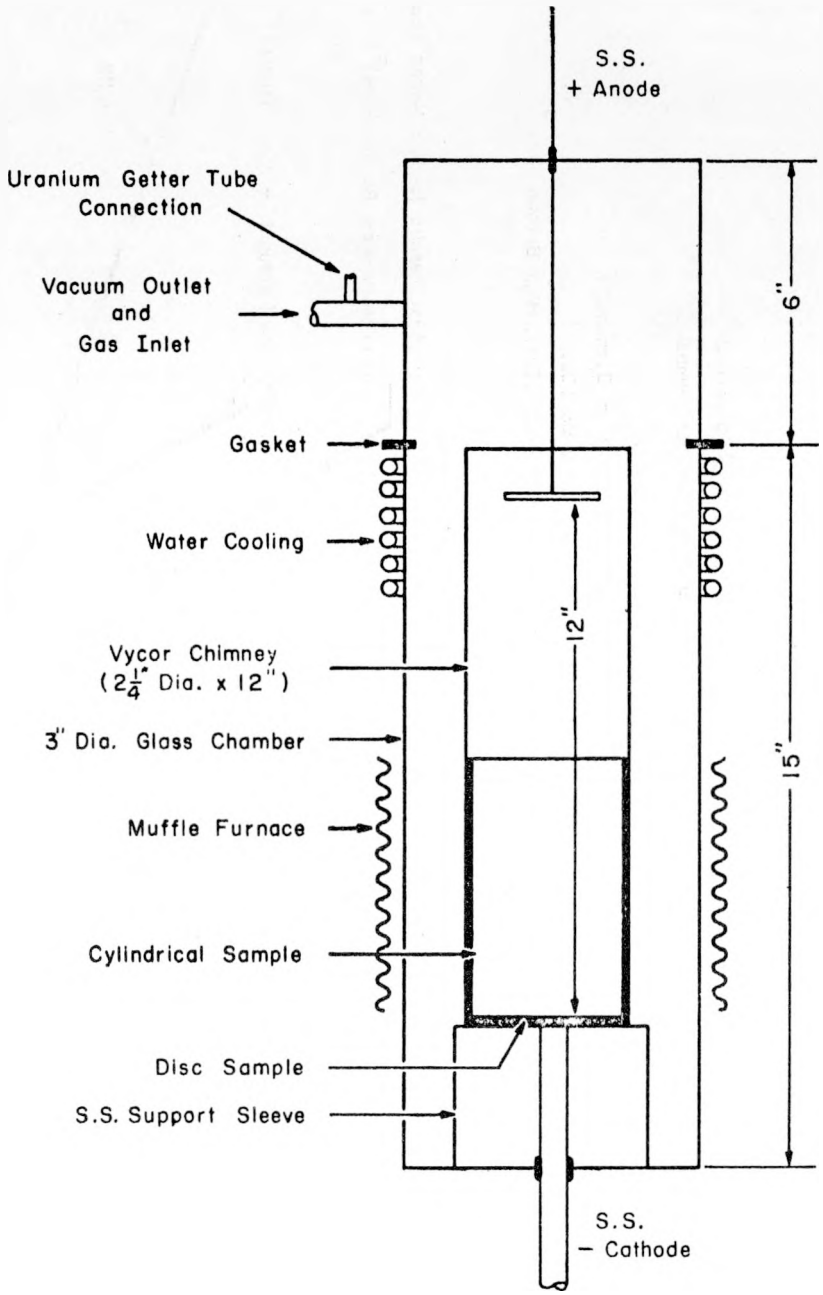

Fig. 2 - Glow-discharge tube.
Drawing No. RA-1617

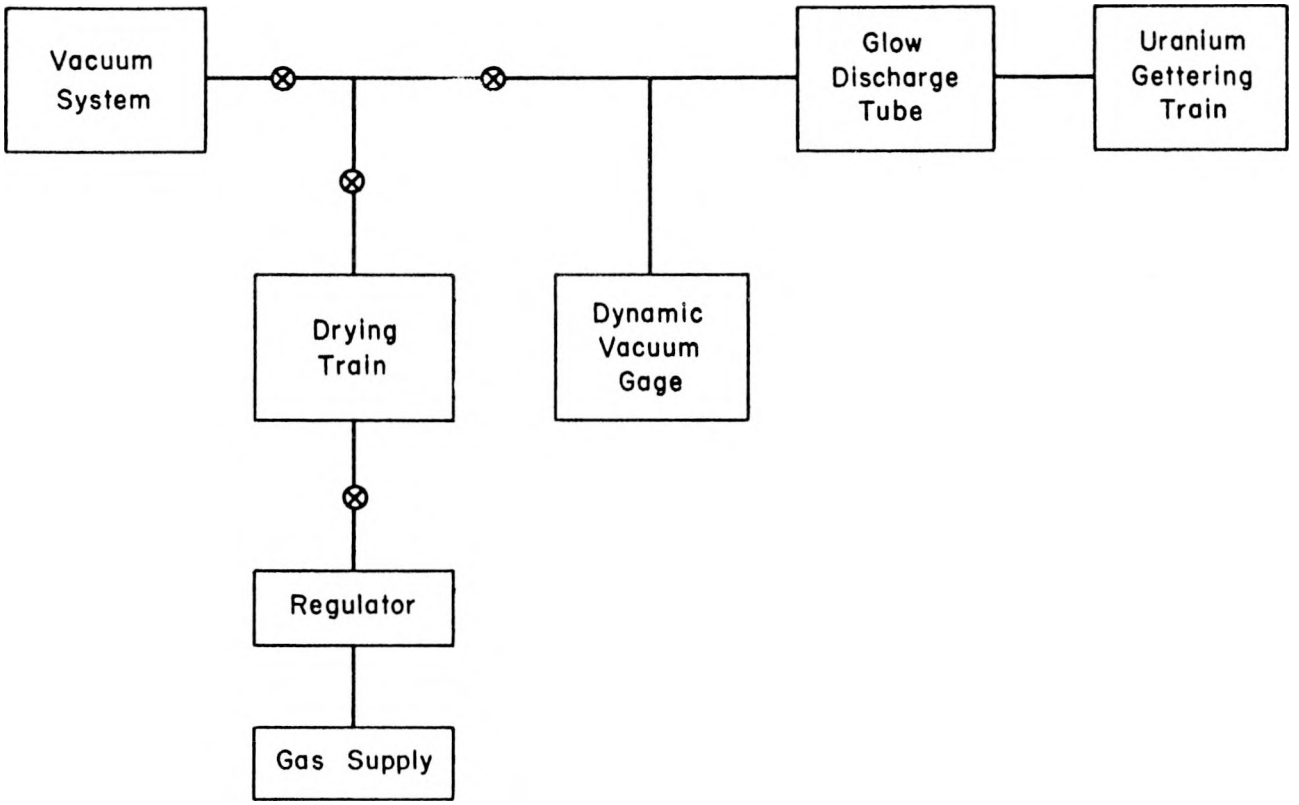

Fig. 3 - Block diagram of glow-discharge apparatus.
Drawing No. RA-1618

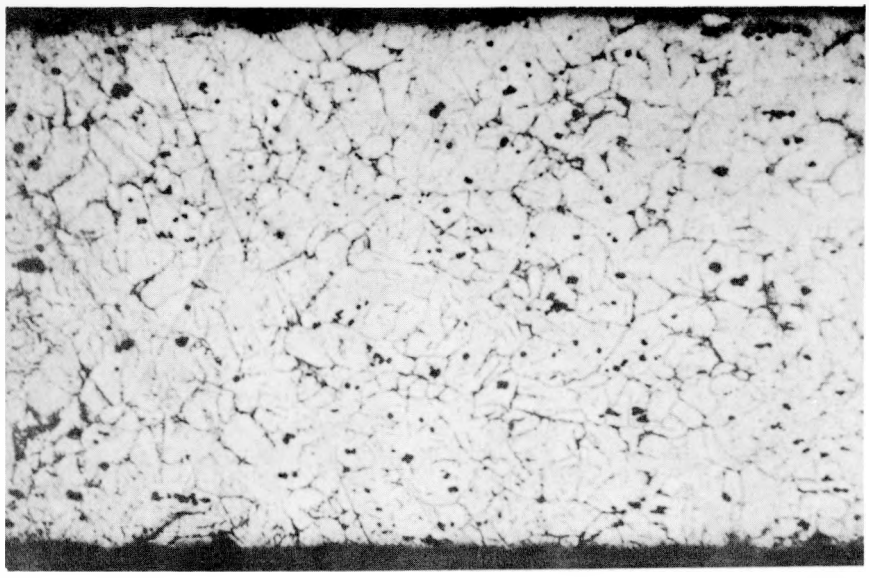

65X Bt. Lt. U-361

Fig. 4 - Cyclotron-irradiated ingot uranium as irradiated.

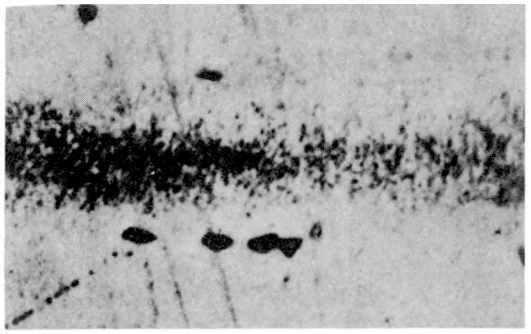

1500X U-379-1a

(a) 90 hr at 600°C

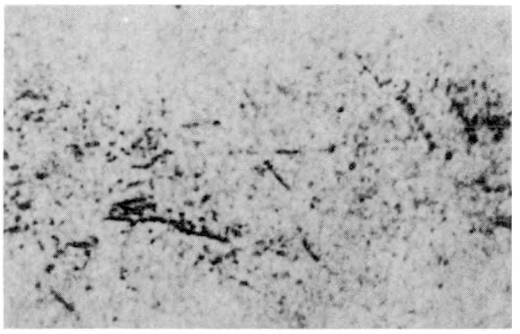

1500X U-380-1a

(b) 90 hr at 730°C

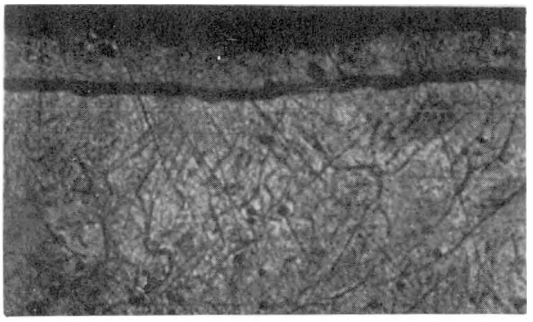

100X U-362-1b

(c) 90 hr at 900°C

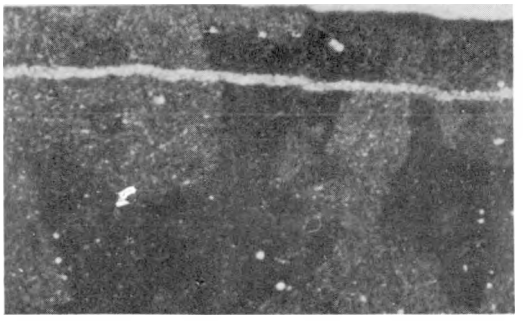

100X Pd. Lt. U-362-1a

(d) 90 hr at 900°C

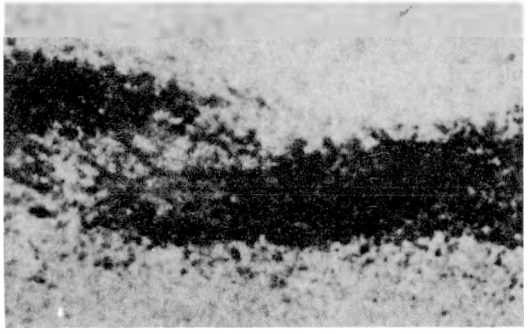

1500X U-362-1c

(e) 90 hr at 900°C

Fig. 5 - Bubble formation in cyclotron-irradiated dingot uranium after various post-irradiation anneals.

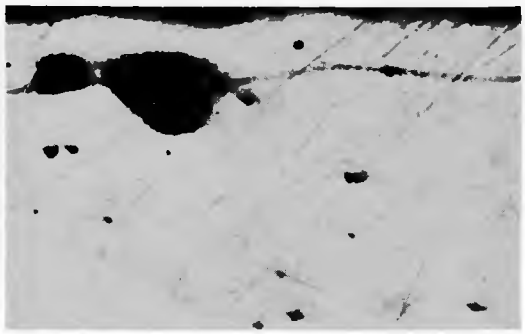

100X U-378-2a

(f) 300 hr at 900°C

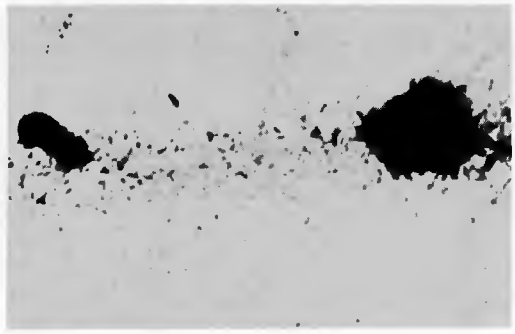

1500X U-378-2b

(g) 300 hr at 900°C

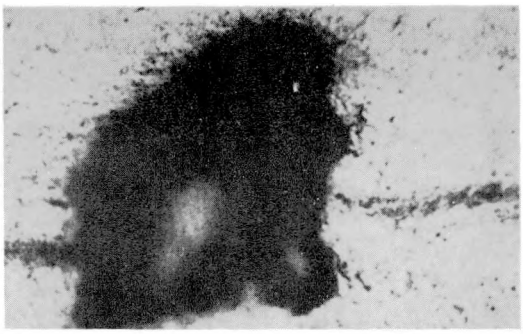

500X U-385-7a

(h) 1000 hr at 900°C

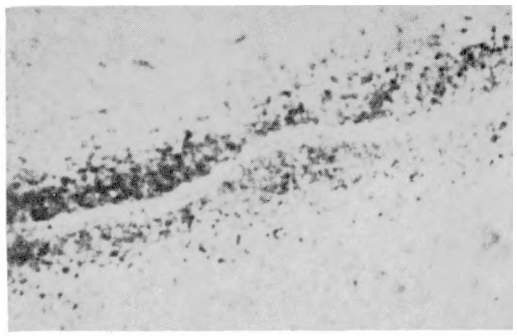

1500X U-385-7b

(i) 1000 hr at 900°C

100X U-372-2a

(j) 90 hr at 975°C

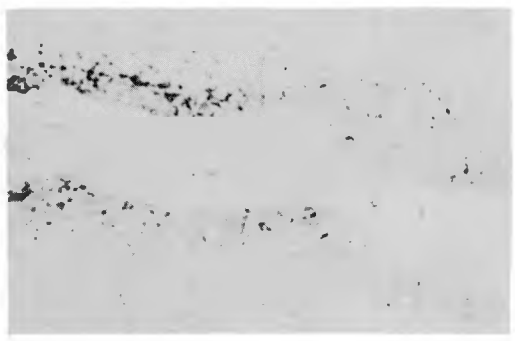

1500X U-372-2b

(k) 90 hr at 975°C

Fig. 5 (Cont'd.) - Bubble formation in cyclotron-irradiated dingot uranium after various post-irradiation anneals.

1500X U-398-3

(a) 2 hr at 1075°C

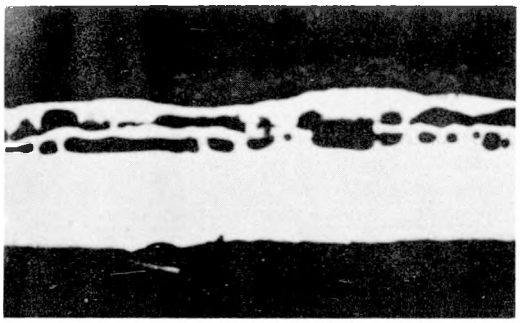

25X U-371-2a

(b) 90 hr at 1075°C

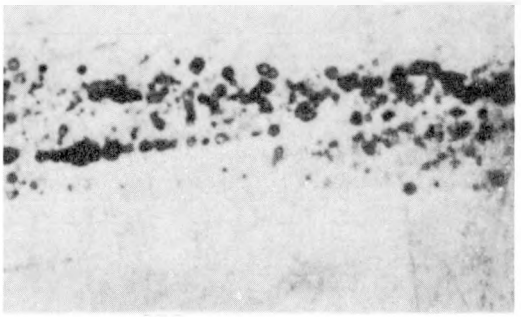

1500X U-371-2e

(c) 90 hr at 1075°C

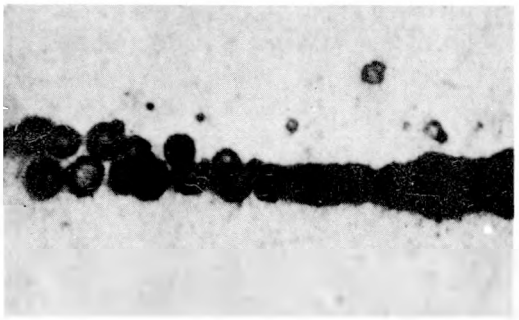

1500X U-371-2c

(d) 90 hr at 1075°C

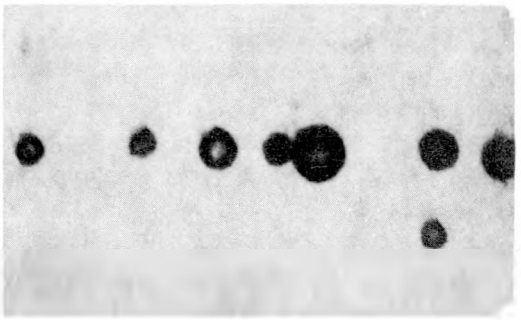

1500X U-371-2d

(e) 90 hr at 1075°C

Fig. 6 - Bubble formation in cyclotron-irradiated dingot uranium after various post-irradiation anneals.

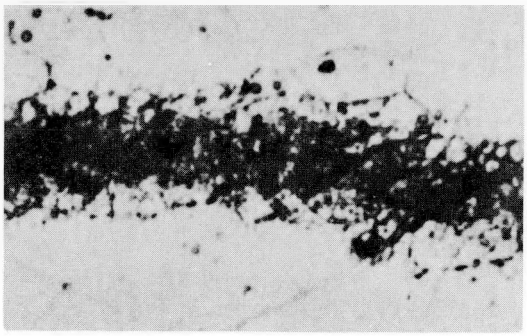

1500X U-379-2a

(a) 90 hr at 600°C

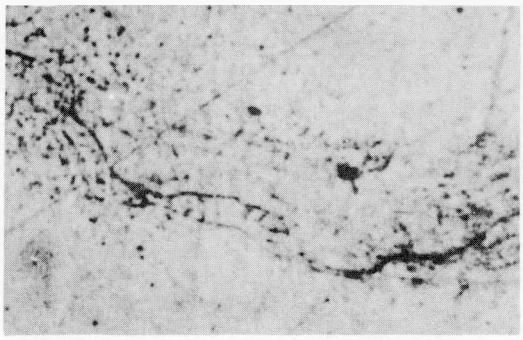

1500X U-380-2

(b) 90 hr at 730°C

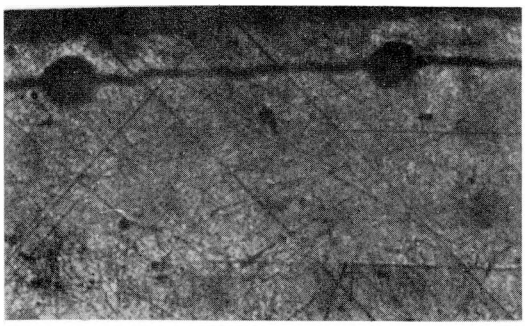

100X U-374-2a

(c) 90 hr at 900°C

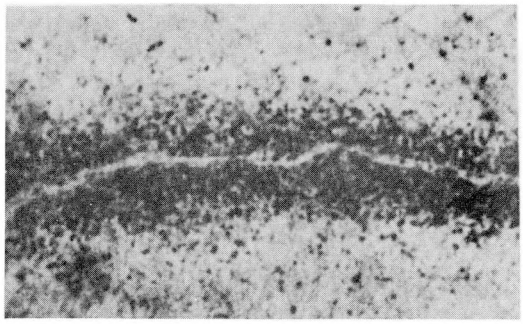

1500X U-374-2b

(d) 90 hr at 900°C

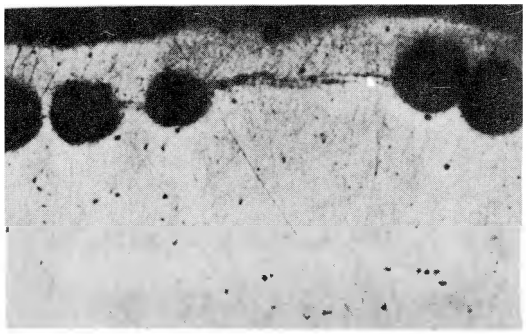

100X U-378-1a

(e) 300 hr at 900°C

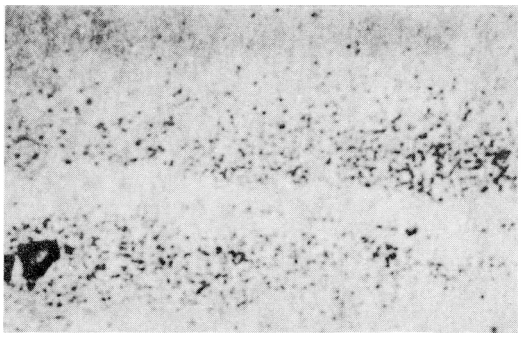

1500X U-378-1b

(f) 300 hr at 900°C

Fig. 7 - Bubble formation in cyclotron-irradiated cold-worked dingot uranium after various post-irradiation anneals.

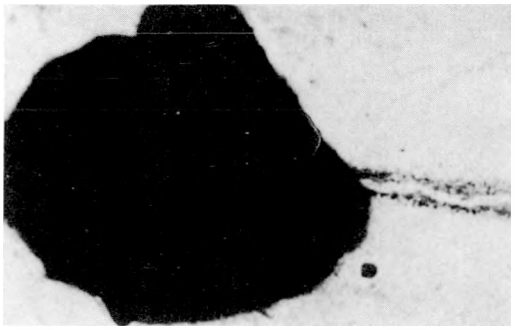

500X U-385-1a

(a) 1000 hr at 900°C

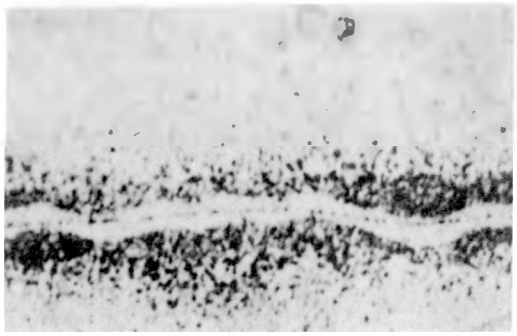

1500X U-385-1b

(b) 1000 hr at 900°C

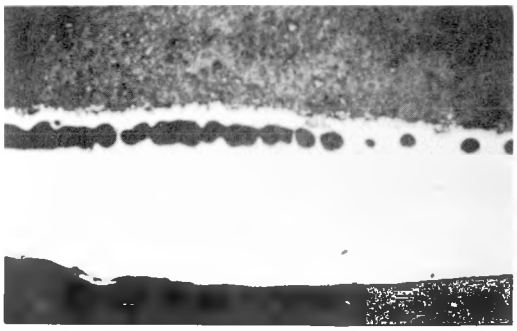

25X U-375-3a

(c) 90 hr at 975°C

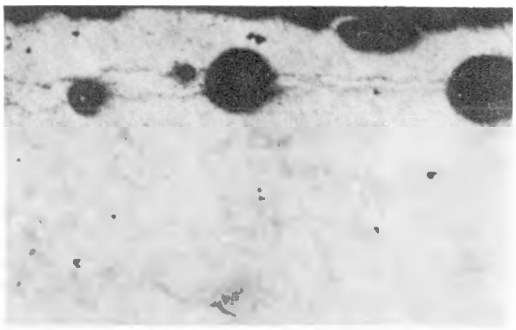

100X U-375-3b

(d) 90 hr at 975°C

1500X U-375-3e

(e) 90 hr at 975°C

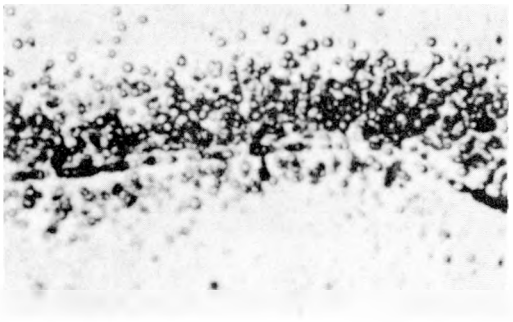

1500X U-383-1a

(f) 90 hr at 1075°C

Fig. 8 - Bubble formation in cyclotron-irradiated cold-worked dingot uranium after various post-irradiation anneals.

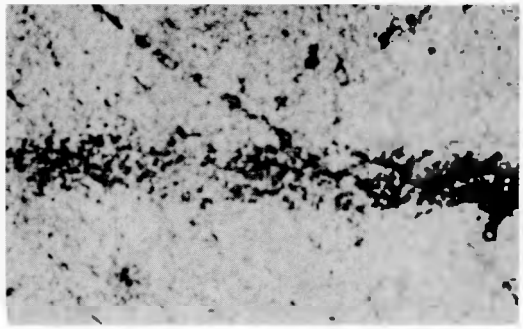

1500X U-367-1b

(a) 20 hr at 550°C, 50 cycles, 550°C for 1 hr, 20°C for 20 min

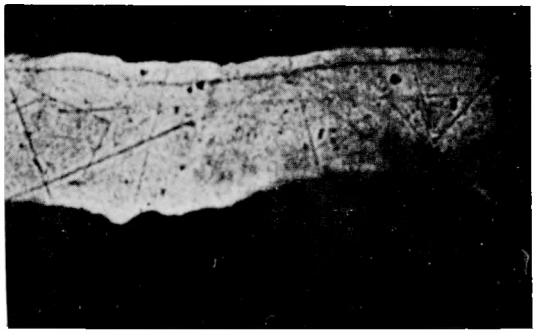

25X U-373-2a

(b) 100 cycles, 730°C for 1 hr, 600°C for 1 hr

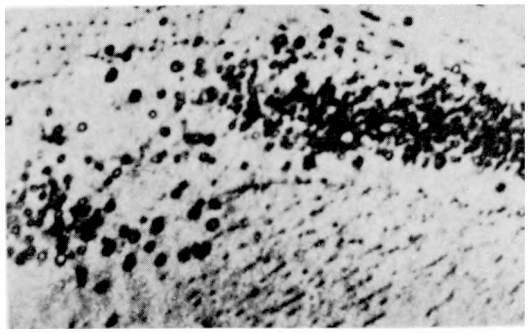

1500X U-373-2b

(c) 100 cycles, 730°C for 1 hr, 600°C for 1 hr

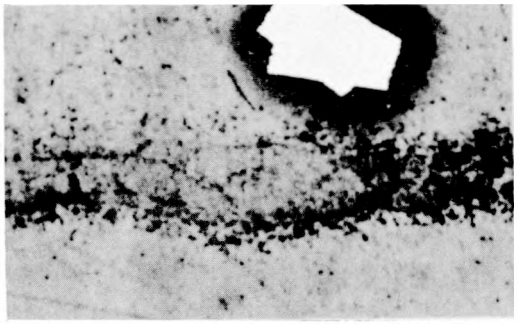

1500X U-370-2a

(d) 10 cycles, 800°C for 1 hr, 475°C for 47 hr

Fig. 9 - Bubble formation in cyclotron-irradiated dingot uranium after various post-irradiation thermal cycling anneals.

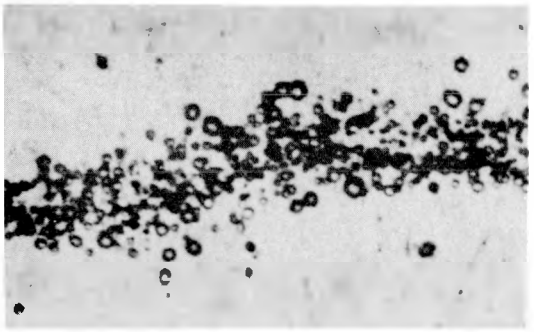

1500X U-386-1a

(a) 100 cycles, 730°C for 1 hr 600°C for 1 hr, 4 hr at 900°C

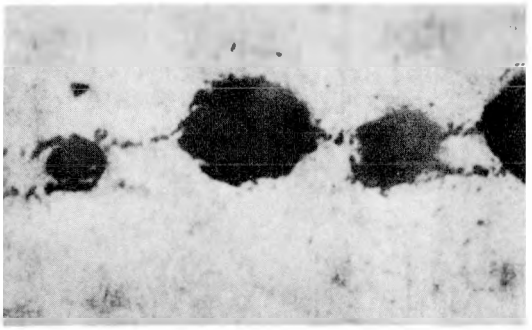

500X U-386-2a

(b) 100 cycles, 730°C for 1 hr, 600°C for 1 hr, 4 hr at 1000°C

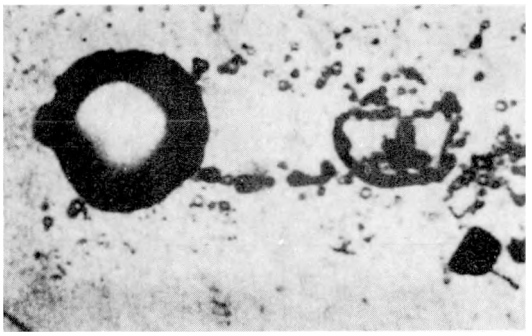

1500X U-386-2d

(c) 100 cycles, 730°C for 1 hr, 600°C for 1 hr, 4 hr at 1000°C

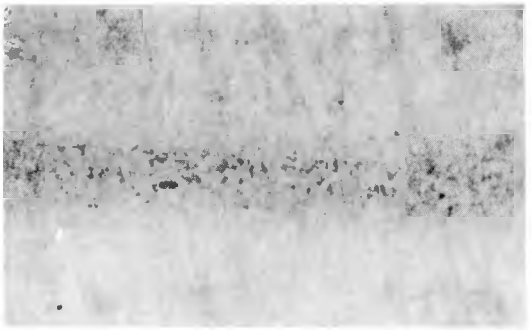

1500X U-392-4a

(d) 25 cycles, 715°C for 10 hr, 600°C for 1-1/2 hr, 90 hr at 900°C

Fig. 10 - Bubble formation in cyclotron-irradiated dingot uranium after various combinations of post-irradiation isothermal and thermal cycling anneals.

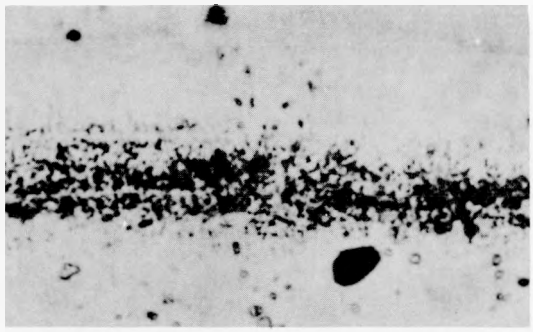

1500X U-379-3

(a) 90 hr at 600°C

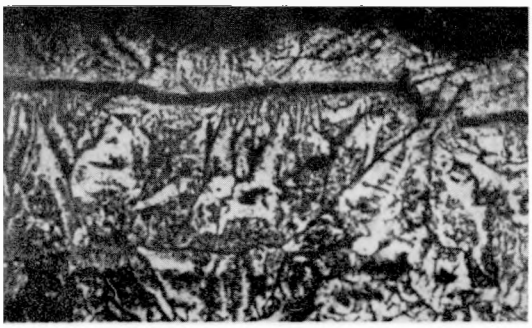

100X U-362-2a

(b) 90 hr at 900°C

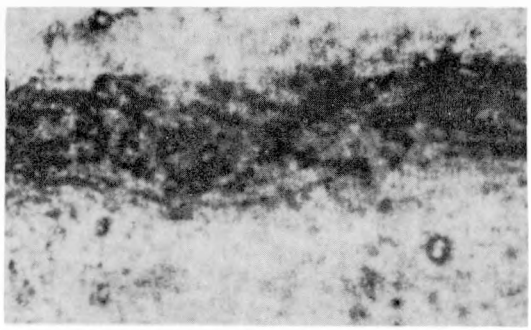

1500X U-362-2b

(c) 90 hr at 900°C

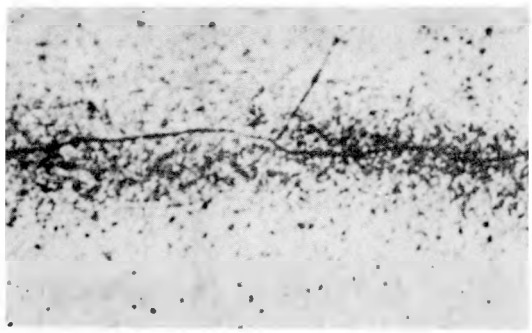

1500X U-385-5a

1000 hr at 900°C

Fig. 11 - Bubble formation in cyclotron-irradiated ingot uranium after various post-irradiation anneals.

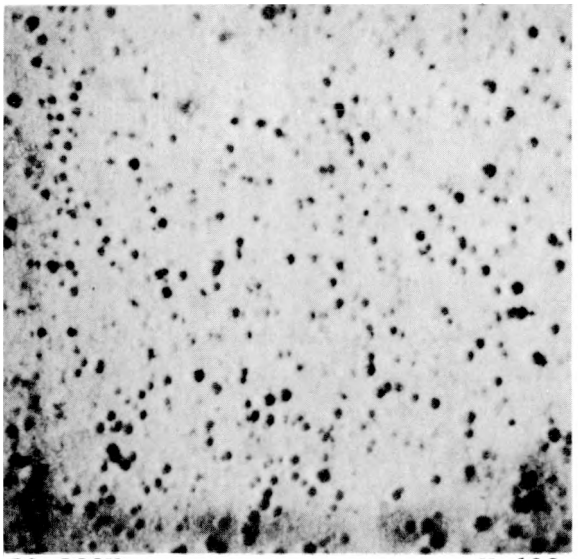

20,000X U-632-2

(a) Dingot uranium

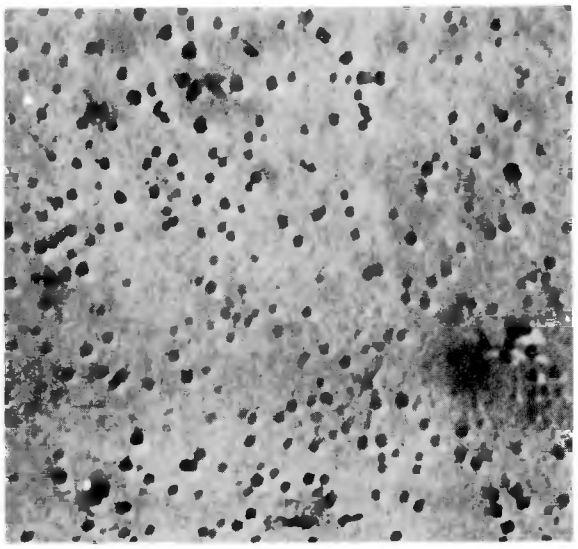

20,000X U-631-g

(b) Ingot uranium

Fig. 12 - Comparison of bubble formation in cyclotron-irradiated ingot and dingot uranium after post-irradiation annealing for 90 hr at 900°C.

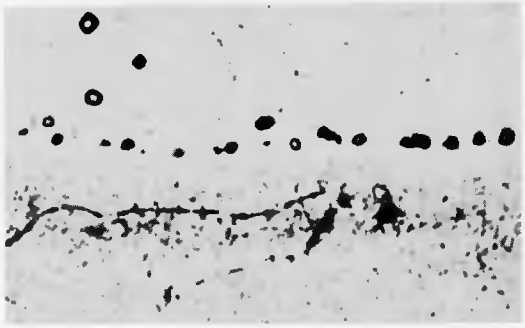

1500X U-372-1a

(a) 90 hr at 975°C

1500X U-398-1

(b) 2 hr at 1075°C

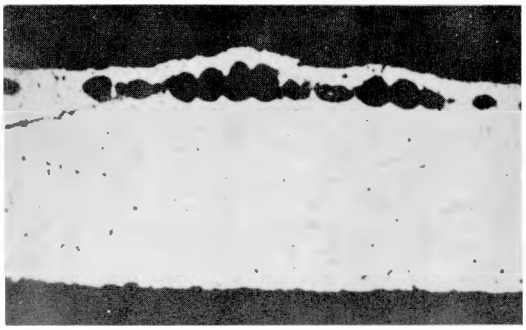

25X U-371-1b

(c) 90 hr at 1075°C

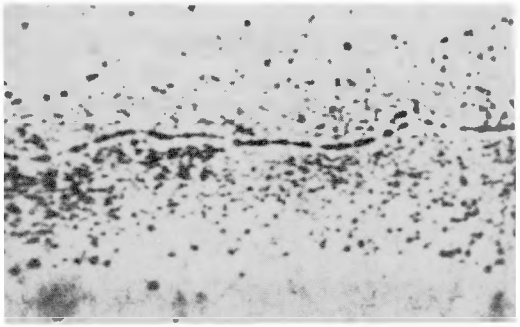

1500X U-371-1c

(d) 90 hr at 1075°C

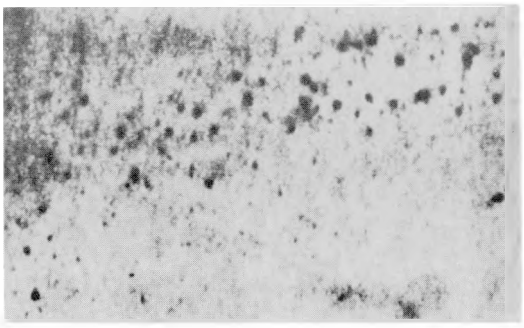

1500X U-371-1e

(e) 90 hr at 1075°C

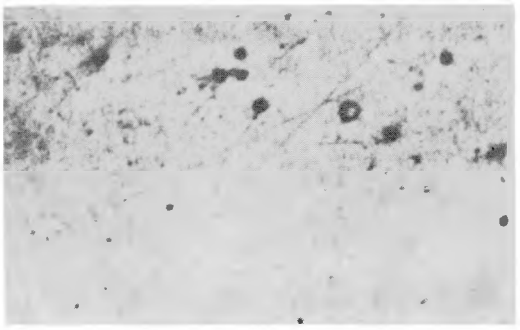

1500X U-371-1f

(f) 90 hr at 1075°C

Fig. 13 - Bubble formation in cyclotron-irradiated ingot uranium after various post-irradiation anneals.

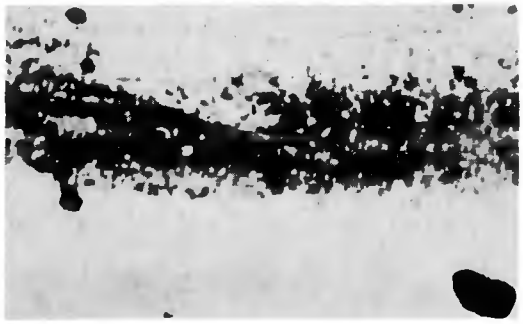

1500X U-379-5a

(a) 90 hr at 600°C

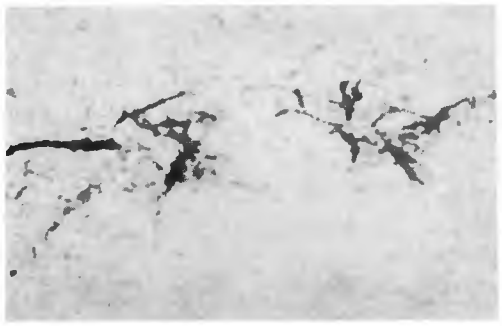

1500X U-380-4a

(b) 90 hr at 730°C

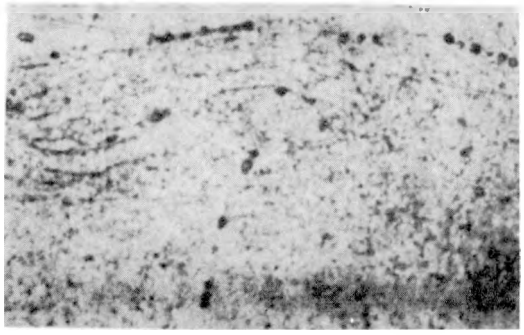

1500X U-374-1b

(c) 90 hr at 900°C

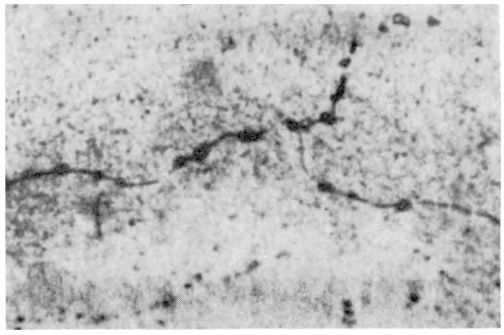

1500X U-377-2b

(d) 300 hr at 900°C

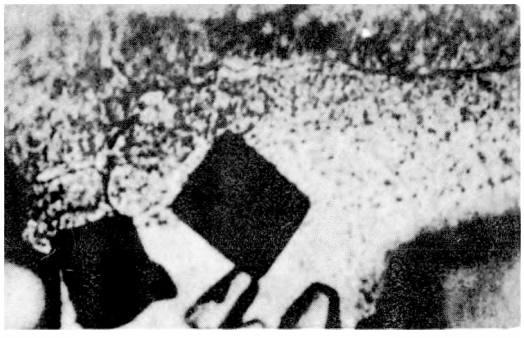

1500X U-385-2b

(e) 1000 hr at 900°C

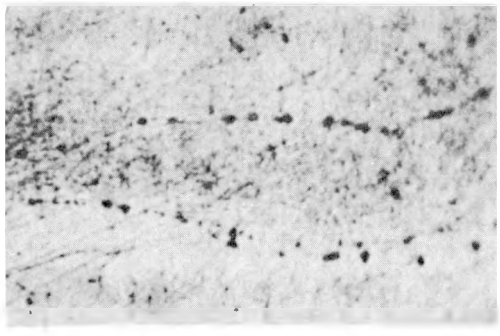

1500X U-375-1b

(f) 90 hr at 975°C

Fig. 14 - Bubble formation in cyclotron-irradiated cold-worked ingot after various post-irradiation anneals.

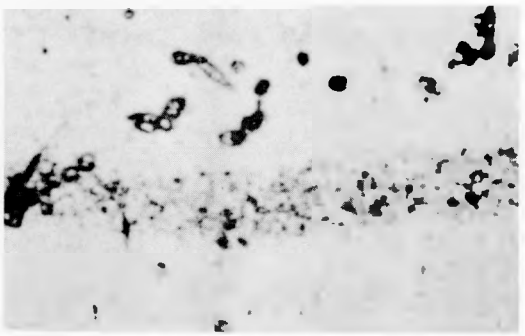

1500X U-367-2b

(a) 50 cycles, 550°C for 1 hr, 20°C for 20 min, 20 hr at 550°C

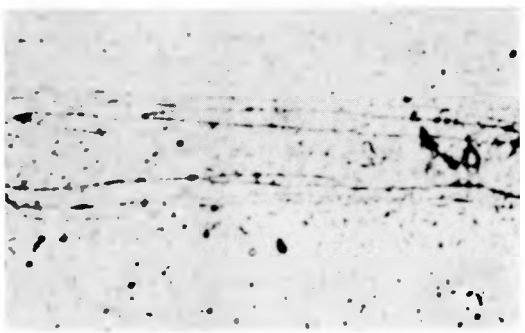

1500X U-370-1b

(b) 10 cycles, 800°C for 1 hr, 475°C for 47 hr

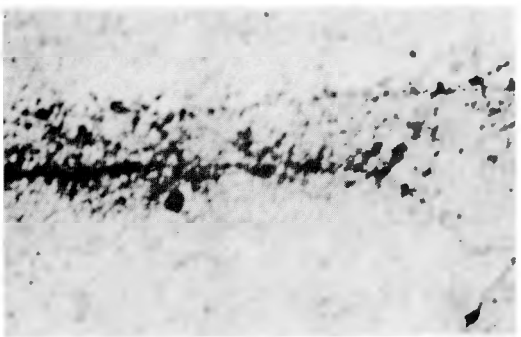

1500X U-373-1a

(c) 100 cycles, 730°C for 1 hr, 600°C for 1 hr.

Fig. 15 - Bubble formation in cyclotron-irradiated ingot uranium after various post-irradiation thermal cycle anneals.

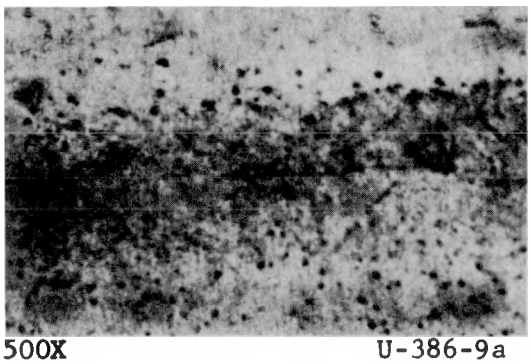

1500X U-386-9a

(a) 100 cycles, 730°C for 1 hr, 600°C for 1 hr, 4 hr at 900°C

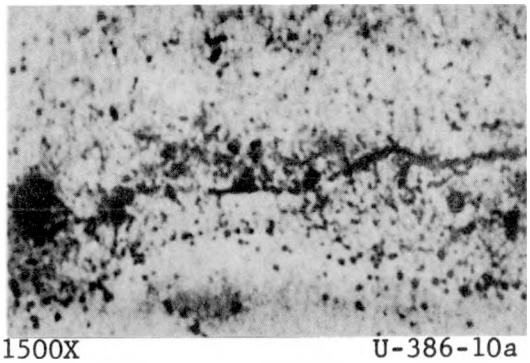

1500X U-386-10a

(b) 100 cycles, 730°C for 1 hr, 600°C for 1 hr, 4 hr at 1000°C

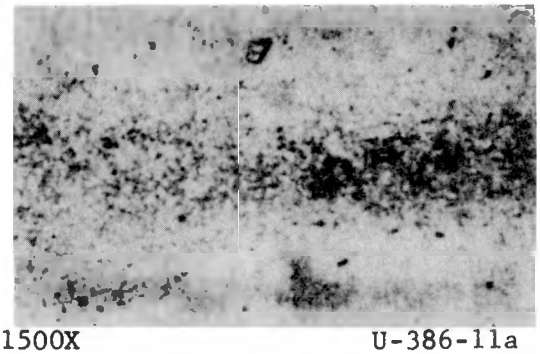

1500X U-386-11a

(c) 100 cycles, 730°C for 1 hr, 600°C for 1 hr, 90 hr at 900°C

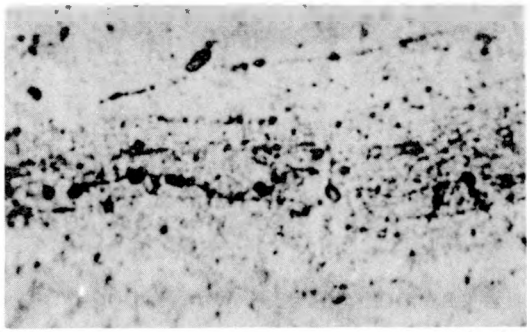

1500X U-396-2

(d) 50 cycles, 550°C for 1 hr, 25°C for 20 min, 90 hr at 900°C

Fig. 16 - Bubble formation in cyclotron-irradiated ingot uranium after various post-irradiation combinations of isothermal and thermal cycle anneals.

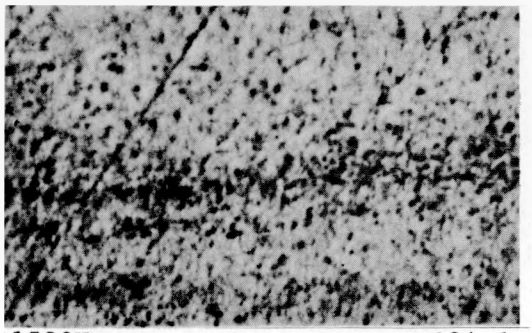

1500X U-384-1a

(a) 16 hr at 550°C

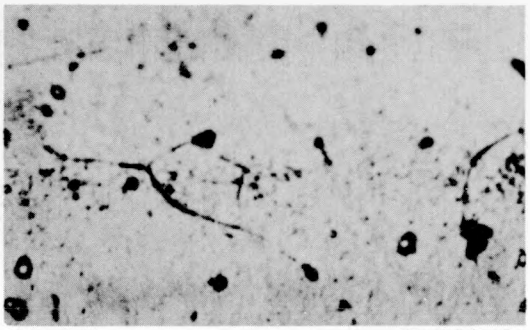

1500X U-384-2a

(b) 10 cycles, 550°C for 1 hr, 25°C for 20 min

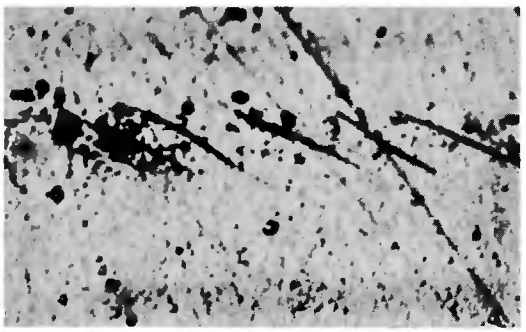

1500X U-384-3a

(c) 10 cycles, 730°C for 1 hr 600°C for 1 hr

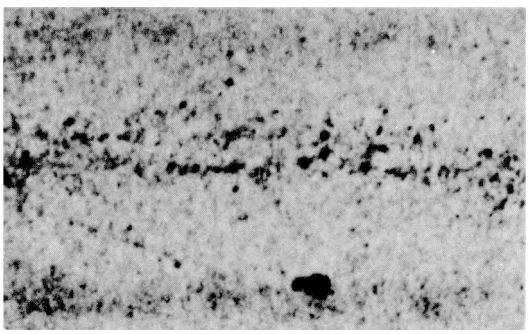

1500X U-384-4a

(d) 16 hr at 900°C

Fig. 17 - Bubble formation in ingot uranium subjected to four intermittent cyclotron-irradiation exposures (7 hr each) and heat treated as noted following each exposure.

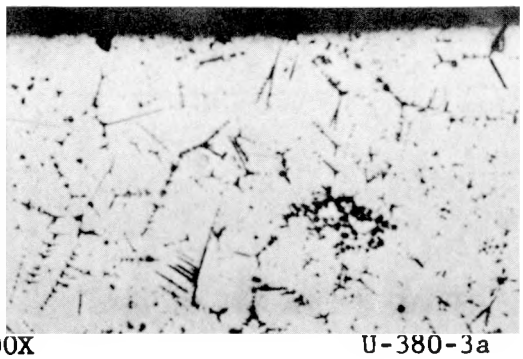

100X U-380-3a

(a) 90 hr at 730°C

1500X U-380-3b

(b) 90 hr at 730°C

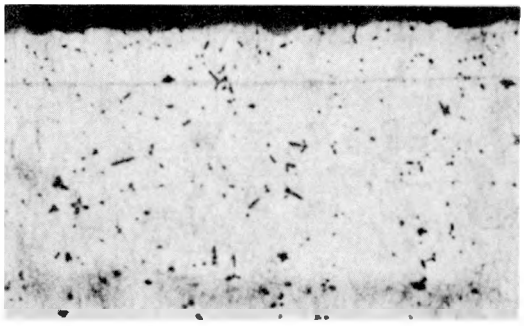

100X U-374-3a

(c) 90 hr at 900°C

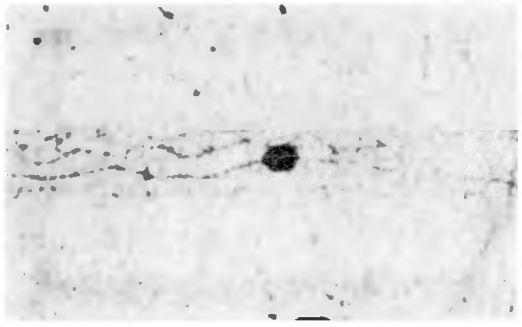

1500X U-374-3b

(d) 90 hr at 900°C

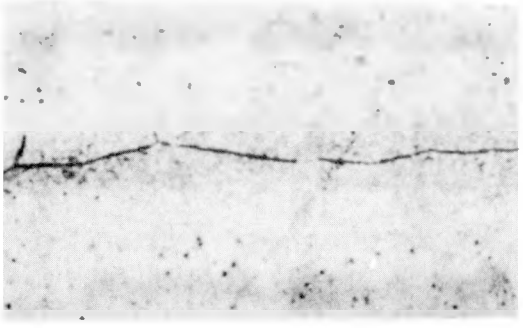

1500X U-377-3b

(e) 300 hr at 900°C

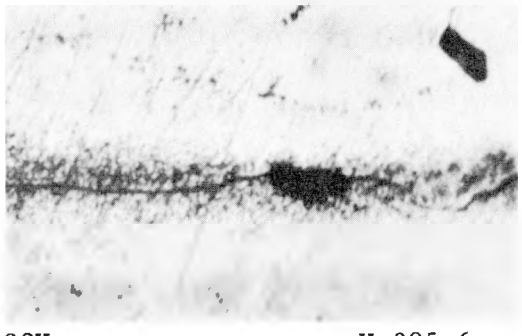

1500X U-385-6a

(f) 1000 hr at 900°C

Fig. 18 - Bubble formation in cyclotron-irradiated arc melted ingot uranium after various post-irradiation anneals.

1500X U-385-4a

Fig. 19 - Bubble formation in cyclotron-irradiated high purity uranium after a post-irradiation anneal. 90 hr at 900°C.

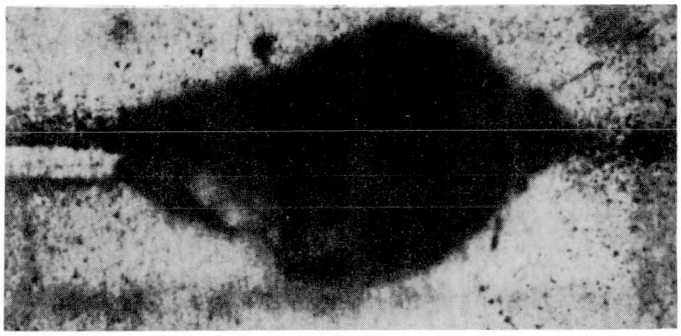

1000X U-386-5a

(a) 100 cycles, 730°C for 1 hr, 600°C for 1 hr, 4 hr at 1000°C

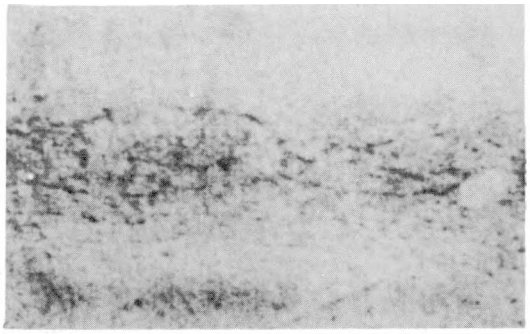

1500X U-386-6a

(b) 100 cycles, 730°C for 1 hr, 600°C for 1 hr, 90 hr at 900°C

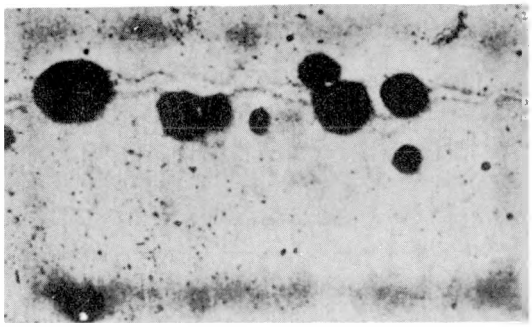

100X U-392-5a

(c) 25 cycles, 715°C for 10 hr, 600°C for 1-1/2 hr, 90 hr at 900°C

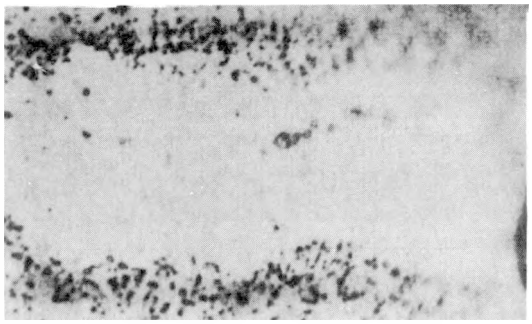

1500X U-392-5b

(d) 25 cycles, 715°C for 10 hr, 600°C for 1-1/2 hr, 90 hr at 900°C

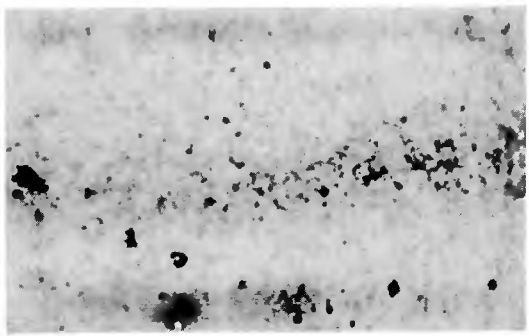

1500X U-392-7

(e) 25 cycles, 715°C for 10 hr, 600°C for 1-1/2 hr, 4 hr at 900°C.

Fig. 20 - Bubble formation in cyclotron-irradiated high purity uranium after various combinations of post-irradiation isothermal and thermal cycle anneals.

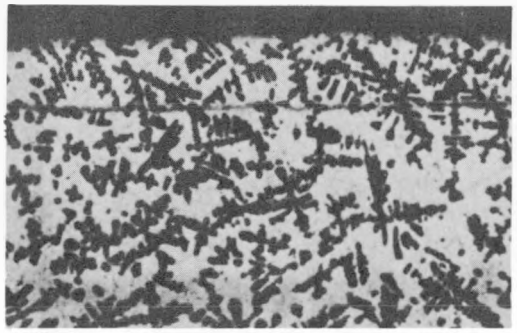

100X A-2830-5a

(a) 300 hr at 900°C

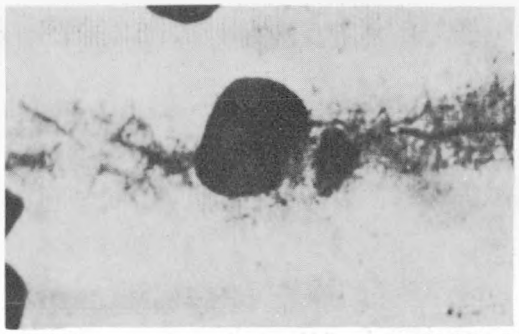

1500X A-2830-5b

(b) 300 hr at 900°C

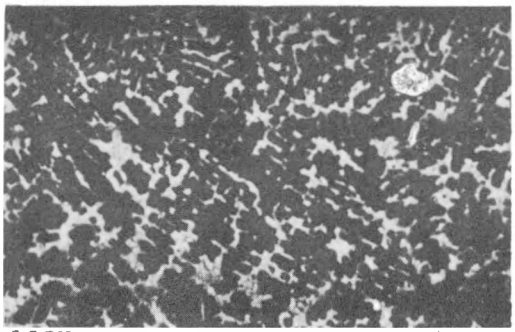

100X A-2830-6a

(c) 300 hr at 900°C

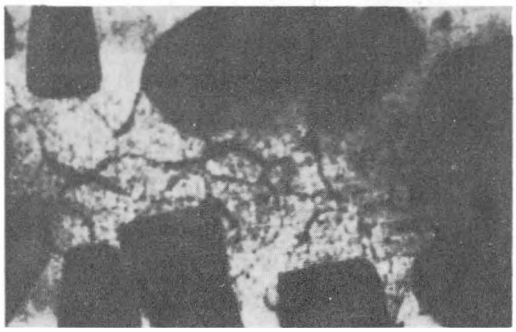

1500X A-2830-6b

(d) 300 hr at 900°C

Fig. 21 - Bubble formation in cyclotron-irradiated uranium-carbon alloys after various post-irradiation anneals. (a) and (b), U - 1 w/o C; (c) and (d), U - 2 w/o C.

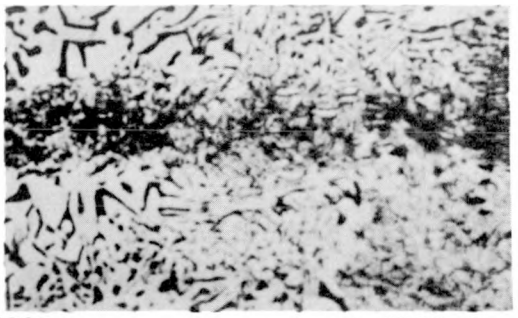

1500X A-2836-2a

(a) 90 hr at 600°C

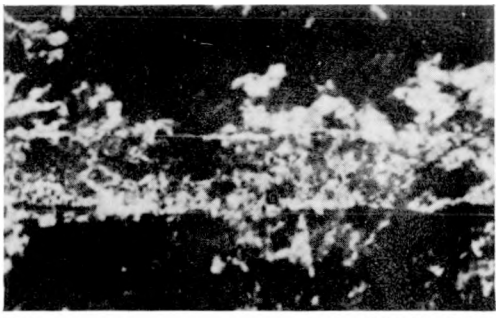

1500X A-2837-10a

(b) 90 hr at 730°C

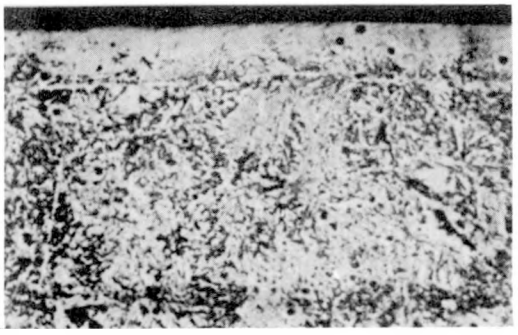

100X A-2813-1b

(c) 90 hr at 900°C

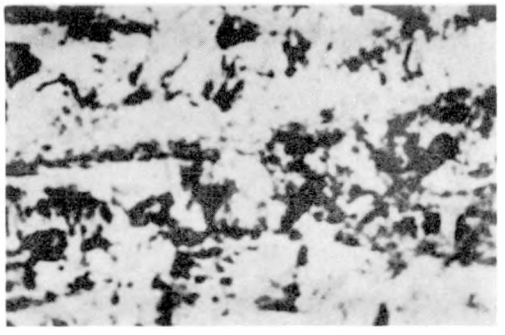

1500X A-2813-1a

(d) 90 hr at 900°C

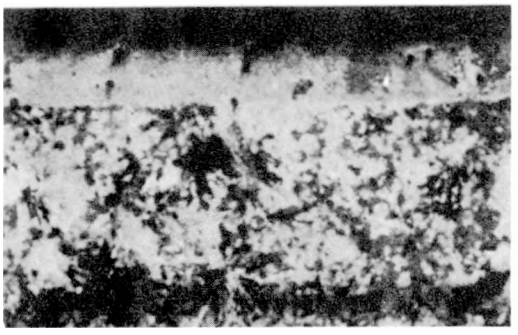

100X A-2830-11a

(e) 300 hr at 900°C

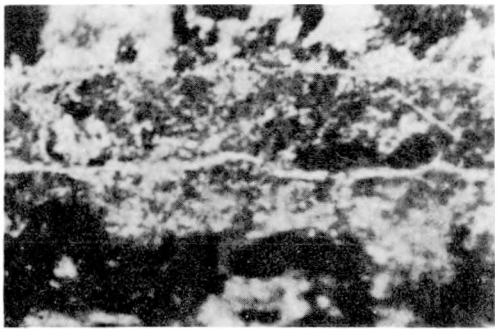

1500X A-2830-11c

(f) 300 hr at 900°C

Fig. 22 - Bubble formation in cyclotron-irradiated U - 1.6 w/o Mo alloy after various post-irradiation anneals.

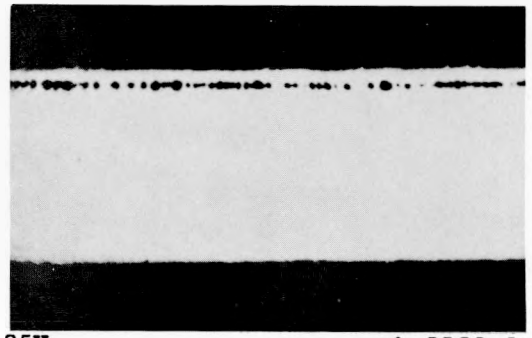

25X A-2823-1c

(g) 90 hr at 975°C

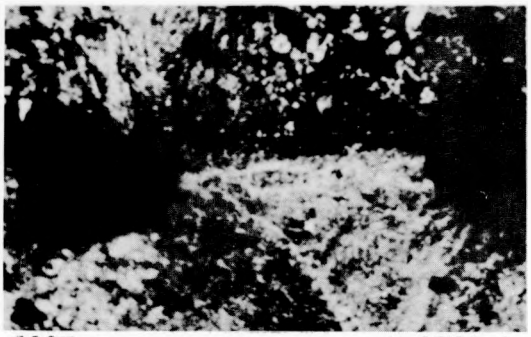

500X A-2823-1a

(h) 90 hr at 975°C

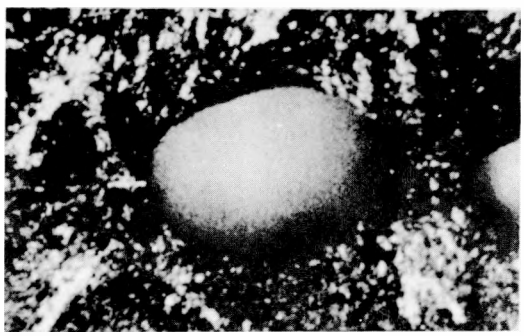

500X A-2860-4a

(i) 90 hr at 1075°C

Fig. 22 (Cont'd.) - Bubble formation in cyclotron-irradiated U - 1.6 w/o Mo alloy after various post-irradiation anneals.

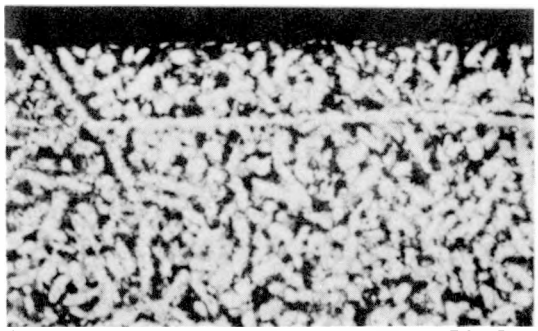

100X A-2874-8a

(a) 25 cycles, 715°C for 10 hr, 600°C for 1 hr

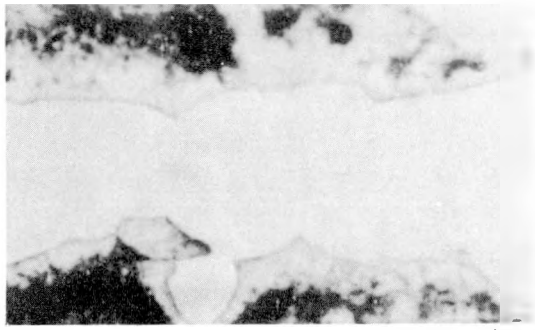

1500X A-2874-8b

(b) 25 cycles, 715°C for 10 hr, 600°C for 1 hr

Fig. 23 - Bubble formation in cyclotron-irradiated U - 1.6 w/o Mo after post-irradiation thermal cycle anneals.

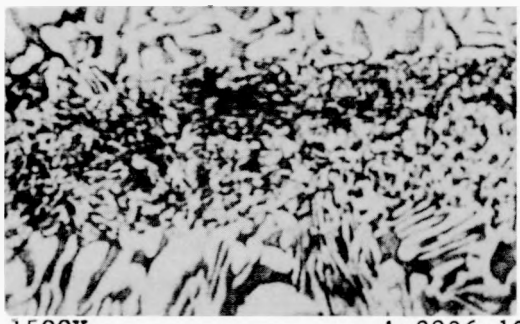

1500X A-2836-10a

(a) 90 hr at 600°C

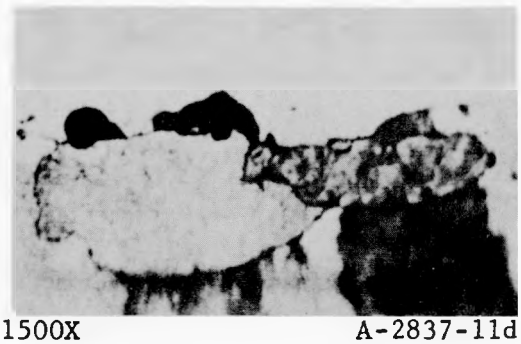

1500X A-2837-11d

(b) 90 hr at 730°C

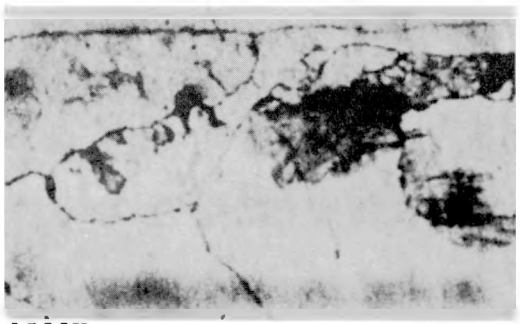

1500X A-2813-2c

(c) 90 hr at 900°C

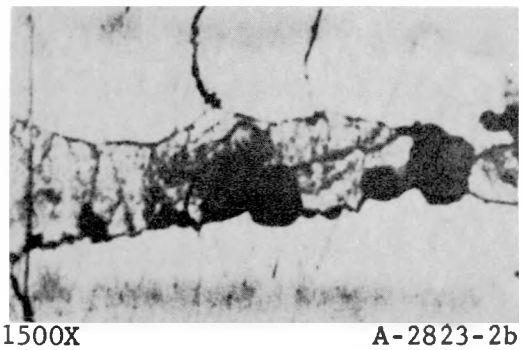

1500X A-2823-2b

(d) 90 hr at 975°C

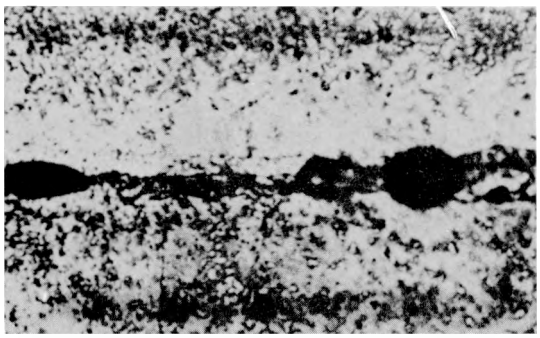

500X A-2890-2

(e) 2 hr at 1075°C

Fig. 24 - Bubble formation in cyclotron-irradiated U - 2.75 w/o Mo after post-irradiation anneals.

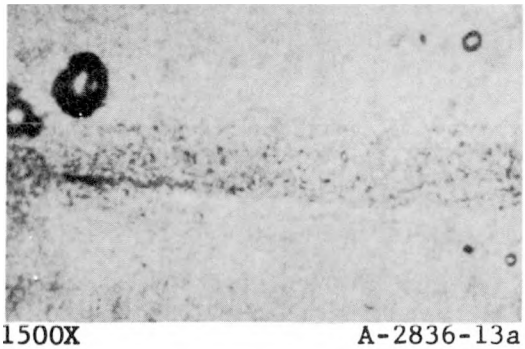

1500X A-2836-13a

(a) 90 hr at 600°C

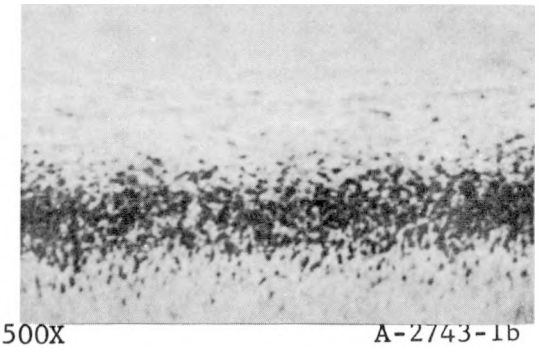

1500X A-2743-1b

(b) 90 hr at 900°C

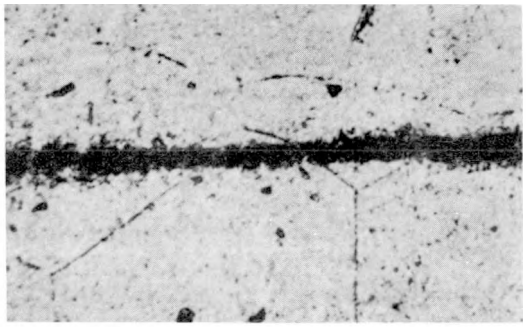

500X A-2792-2a

(c) 90 hr at 975°C

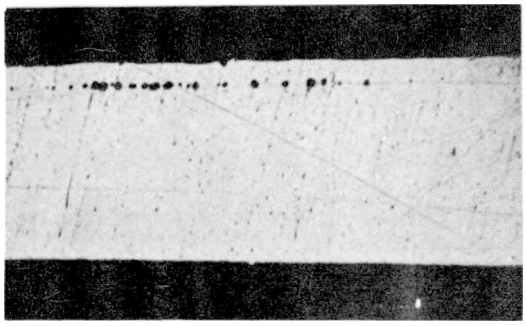

25X A-2791-2a

(d) 90 hr at 1075°C

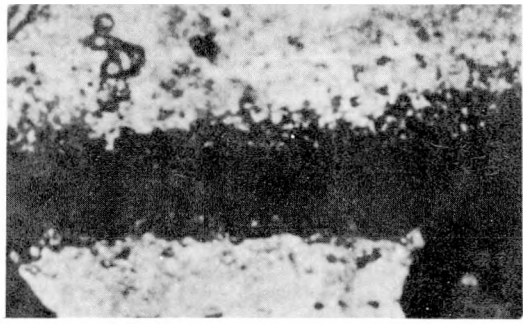

1500X A-2791-2b

(e) 90 hr at 1075°C

Fig. 25 - Bubble formation in cyclotron-irradiated retained gamma phase U - 10 w/o Mo after various post-irradiation anneals.

1500X A-2761-1a

(a) 50 cycles, 550°C for 1 hr, 20°C for 20 min, 20 hr at 550°C

1500X A-2761-1c

(b) 50 cycles, 550°C for 1 hr, 20°C for 20 min, 20 hr at 550°C

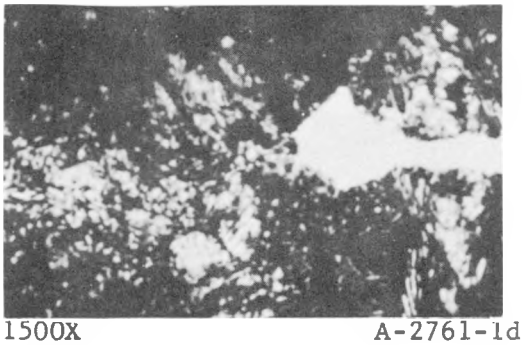

1500X A-2761-1d

(c) 50 cycles, 550°C for 1 hr, 20°C for 20 min, 20 hr at 550°C

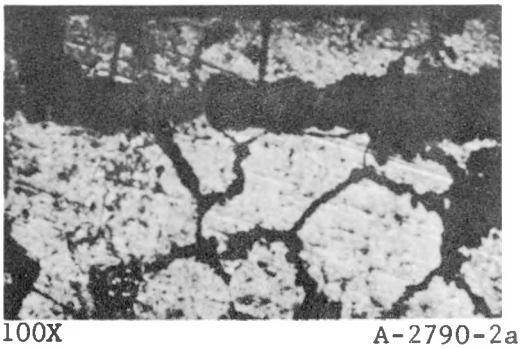

100X A-2790-2a

(d) 10 cycles, 800°C for 1 hr, 475°C for 47 hr.

Fig. 26 - Bubble formation in cyclotron-irradiated U - 10 w/o Mo after various post-irradiation thermal cycle anneals.

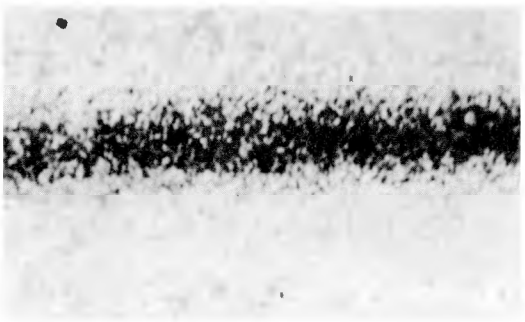

1500X A-2879-3

25 cycles, 715°C for 10 hr, 600°C for 1-1/2 hr, 4 hr at 900°C

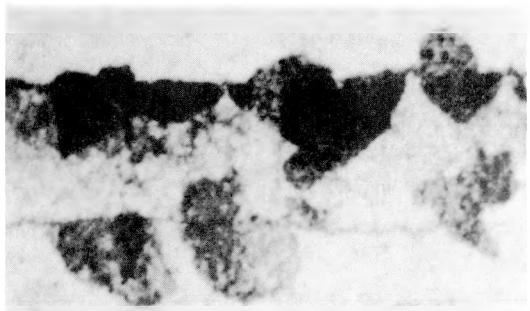

1500X A-2863-7a

100 cycles, 730°C for 1 hr, 600°C for 1 hr, 90 hr at 900°C

Fig. 27 - Bubble formation in cyclotron-irradiated U - 10 w/o Mo after various post-irradiation isothermal and thermal cycling anneals.

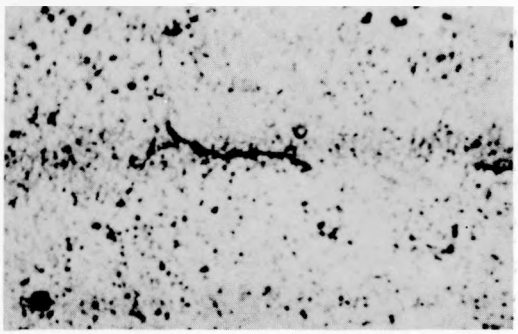

1500X A-2836-1a

(a) 90 hr at 600°C

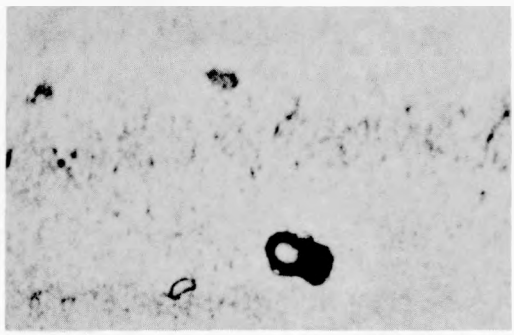

1500X A-2837-1a

(b) 90 hr at 750°C

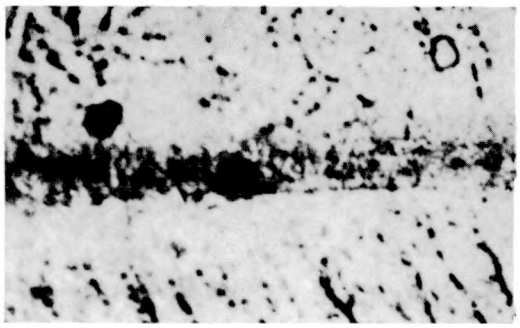

1500X A-2814-a

(c) 90 hr at 900°C

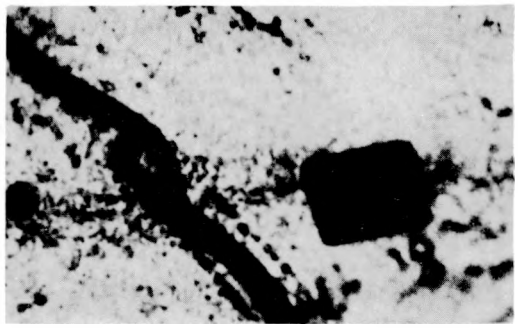

1500X A-2830-4a

(d) 300 hr at 900°C

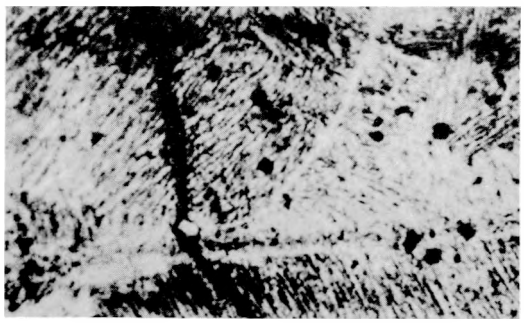

1500X A-2879-a

(e) 90 hr at 975°C

Fig. 28 - Bubble formation in cyclotron-irradiated beta phase U - 0.3 w/o Mo - 0.3 w/o Cr after various post-irradiation anneals.

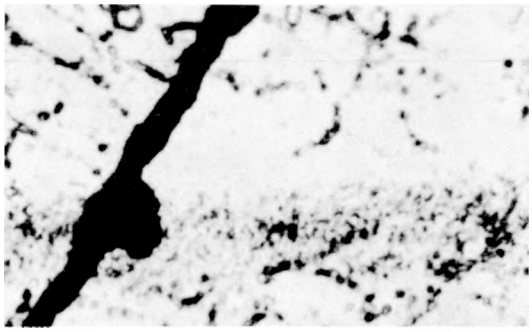

1500X A-2879-5

Fig. 29 - Bubble formation in cyclotron-irradiated beta phase U - 0.3 w/o Mo - 0.3 w/o Cr after a post-irradiation thermal-cycle anneal. 25 cycles, 715°C for 10 hr, 600°C for 1 hr, 4 hr at 900°C.

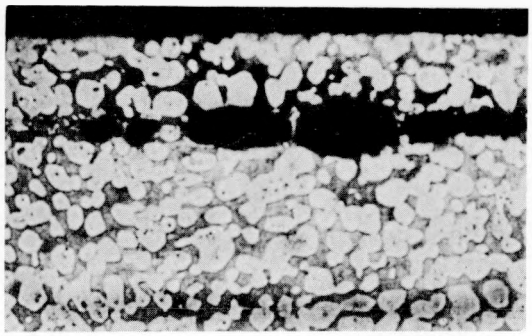

100X A-2830-8a

(a) 300 hr at 900°C

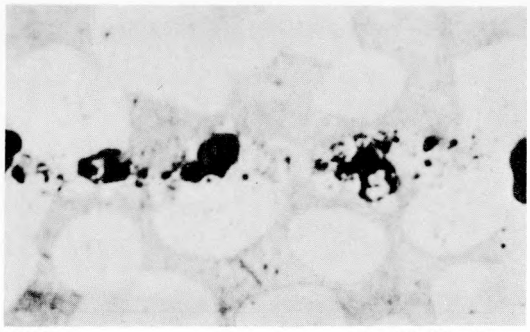

500X A-2830-8c

(b) 300 hr at 900°C

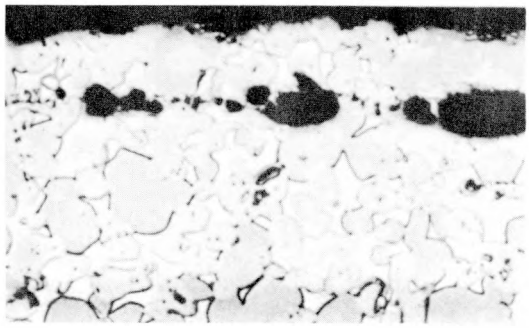

100X A-2861-3a

(c) 1000 hr at 900°C

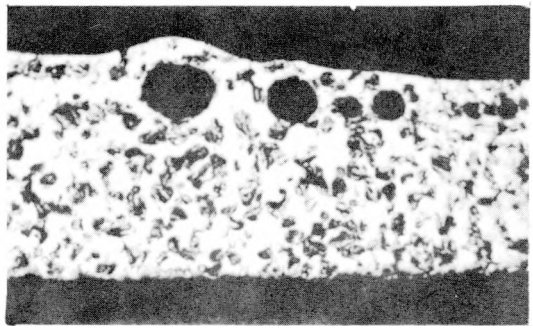

25X A-2821-1a

(d) 90 hr at 975°C

Fig. 30 - Bubble formation in cyclotron-irradiated U - 3.8 w/o Si after various post-irradiation anneals.

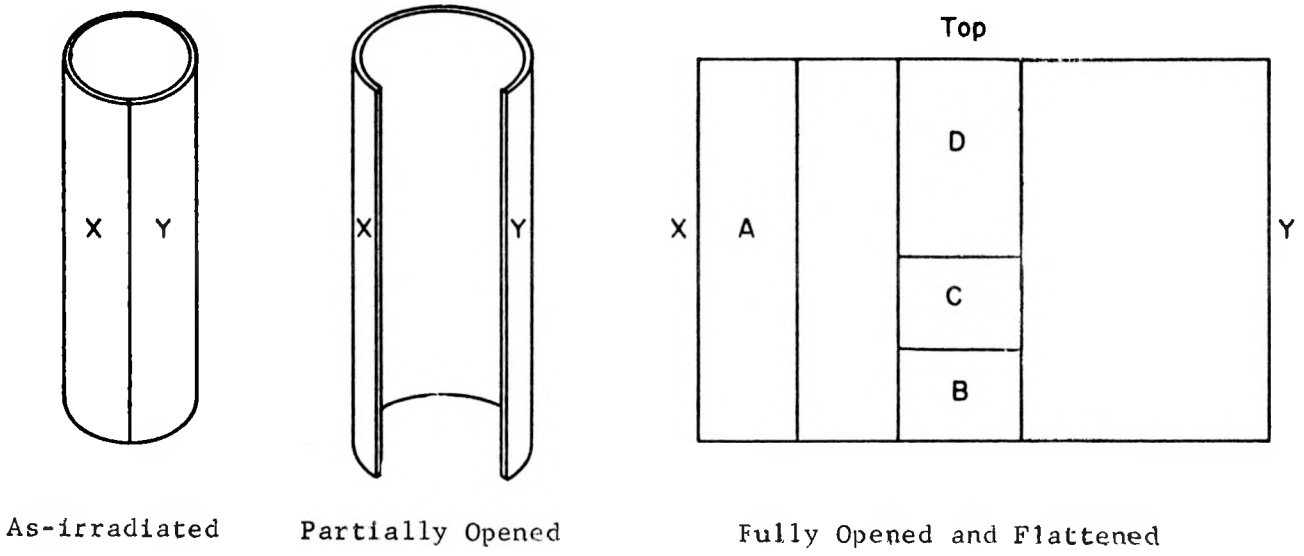

Fig. 31 - Position of samples with respect to original cathode. Drawing No. RA-1619

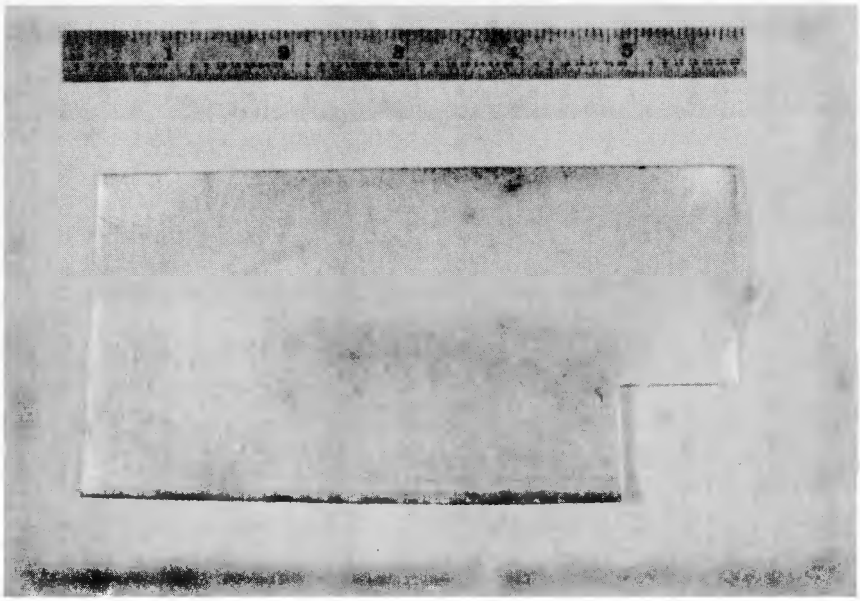

RF-7481

Fig. 32 - Fully opened copper glow-discharge sample showing two distinct bands. It also contains large surface bubbles not typical of all samples.

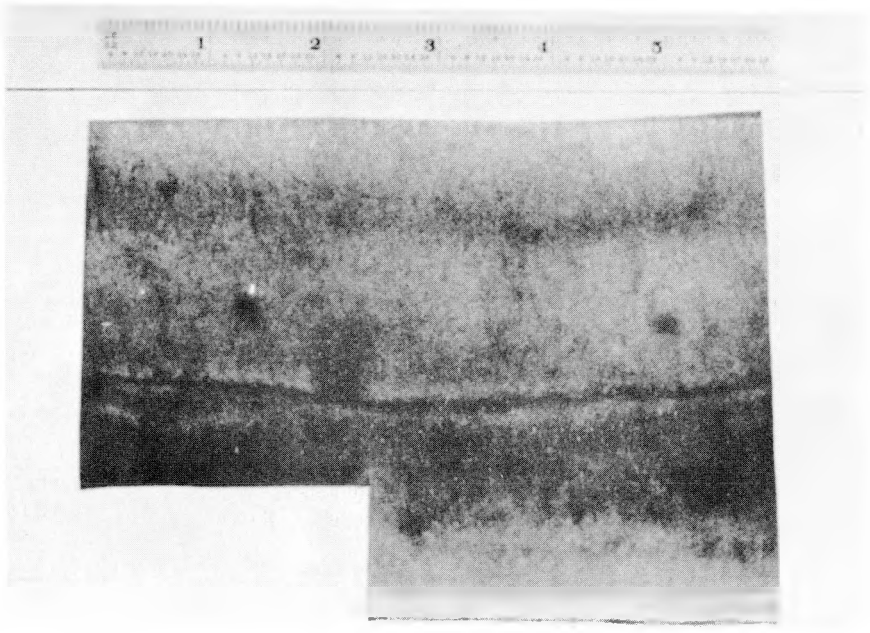

RF-7480

Fig. 33 - Fully opened uranium glow-discharge sample showing multiple bands. Induced gas was concentrated in bands near the top.

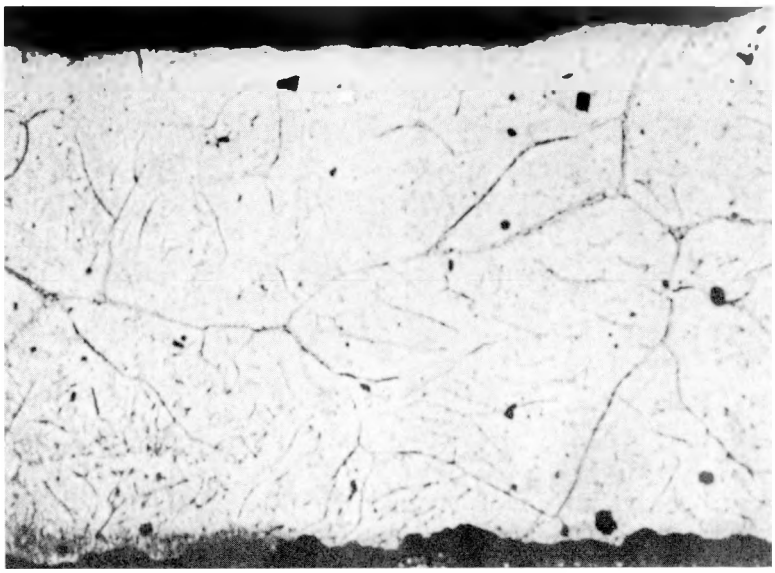

250X U-390-2a

Fig. 34 - Uranium exposed to krypton in the glow-discharge unit, run GD-9, after a post-glow anneal. 90 hr at 900°C

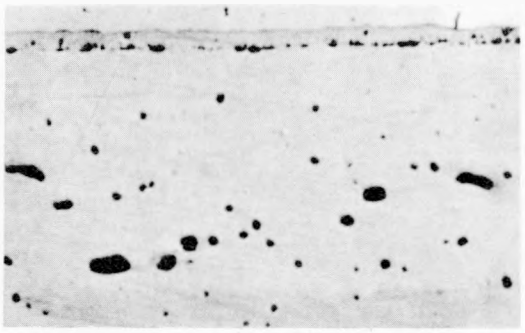

100X A-2870-3a

(a) 90 hr at 900°C

1500X A-2870-4d

(b) 90 hr at 900°C

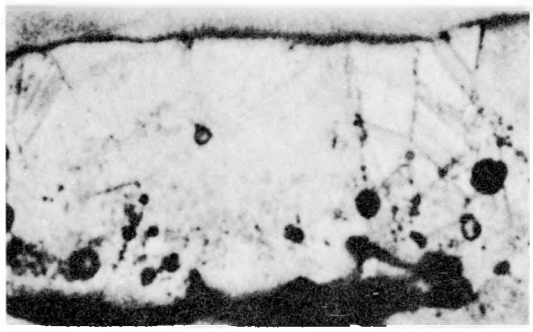

1500X A-2870-3g

(c) 90 hr at 900°C

Fig. 35 - Copper exposed to krypton in the glow-discharge unit, run GD-7 after post-glow anneals.

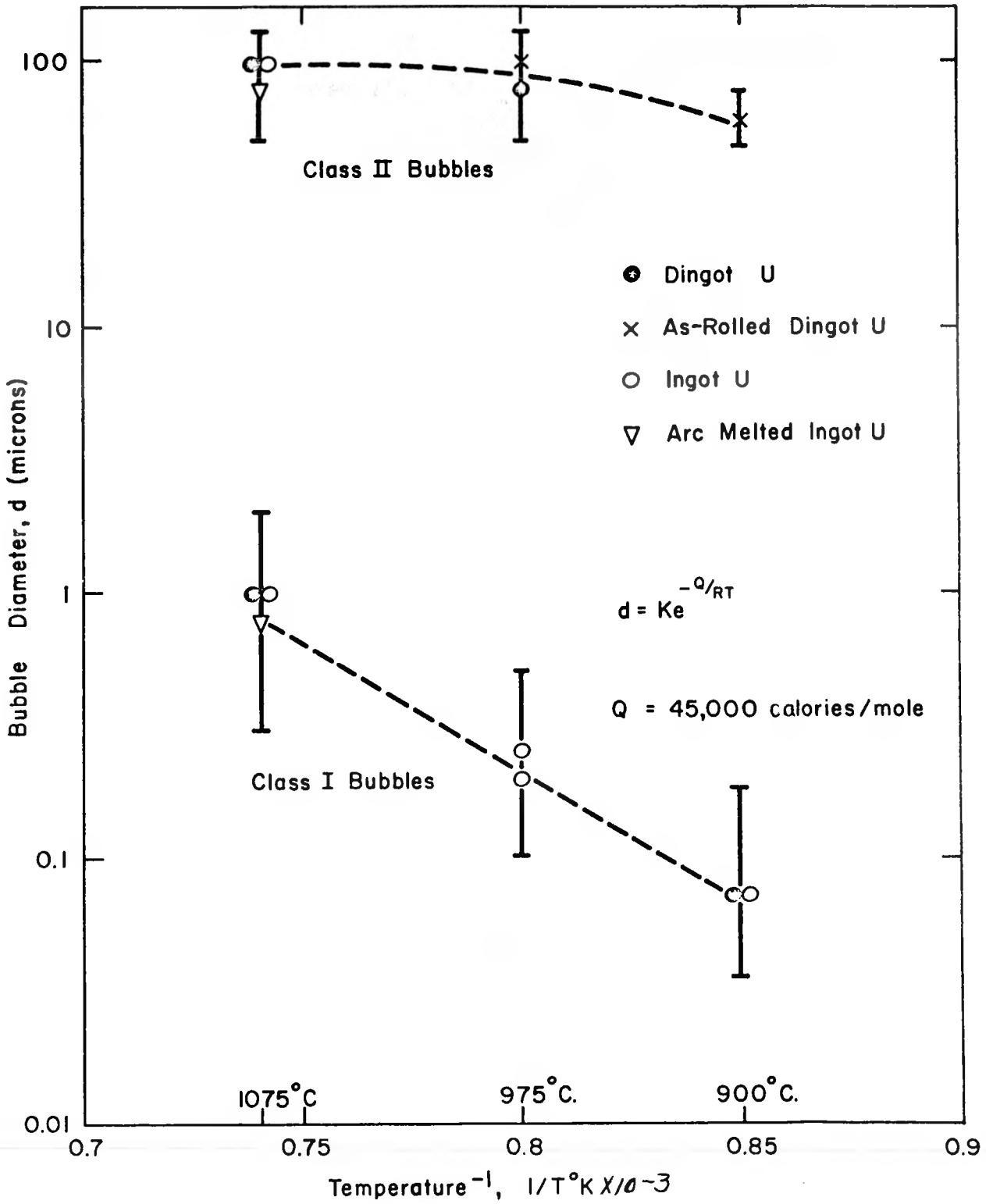

Fig. 36 - Gas bubble diameter vs annealing temperature of cyclotron-irradiated uranium annealed for 90 hr at the indicated temperatures. Drawing No. RA-1653

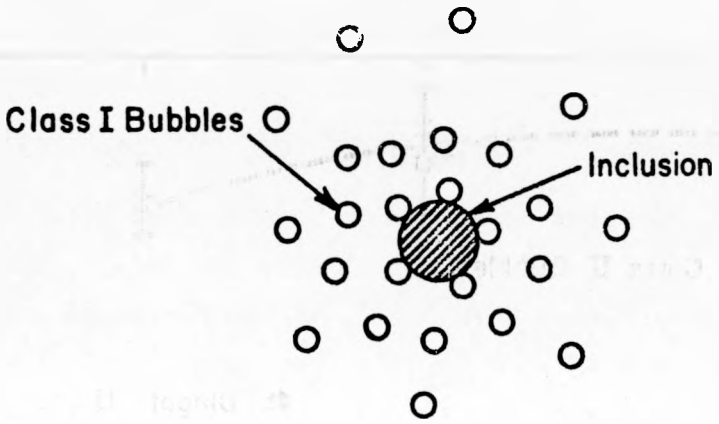

A. Behavior of Class I Bubbles at Low Temp.

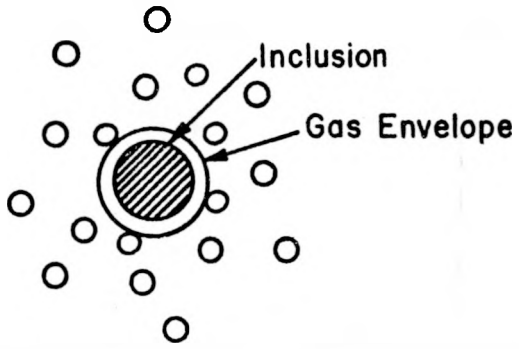

B. Transformation or Loss of Coherency

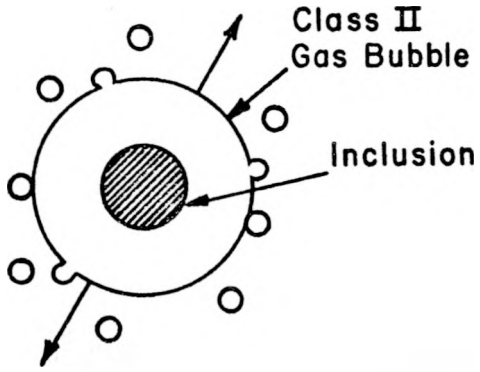

C. Catastrophic Growth Stage

Fig. 37 - Schematic illustration of hypothetical mechanism for the formation of Class II bubbles. Drawing No. RA-1652

VII. REFERENCES

1. R. S. Barnes, Nuclear Metallurgy, Vol. VI, AIME Pub., 1959, 21.

2. J. B. Rich, G. B. Redding, and R. S. Barnes, Journal of Nuclear Materials, 1, 1959.

3. C. E. Ells and W. Evans, CR-Met-863, Atomic Energy of Canada, Ltd., 1959.

4. C. E. Ells and W. Evans, CR-Met-864, Atomic Energy of Canada, Ltd., 1959.

5. A. Boltax, NMI-7001, 1960, SECRET (To be prepared as an unclassified report).

6. A. D. LeClaire and A. H. Rowe, AERE-M/R-1417, U. K. Atomic Energy Authority, 1954.

7. J. M. Tobin, HW-53639, 1958.

8. R. S. Barnes, et al., 1958, Geneva Conference, No. 81.

9. A. T. Churchman, Nuclear Metallurgy, Vol. VI, AIME Pub., 1959, 13.

10. A. Robillard, CEA-1057, French Atomic Energy Commission, 1959.

11. J. Greenspan, 1960, AEC Annual Report, NMI, 1960.

12. H. Green, NMI-7222, June 23, 1960, p. 19.

13. D. E. Thomas, et al., 1958, Geneva Conference, No. 1924.